© 2020. Published by The Company of Biologists Ltd | Journal of Cell Science (2020) 133, jcs237990. doi:10.1242/jcs.237990

RESEARCH ARTICLE

Distinct roles of two eIF4E isoforms in the germline of *Caenorhabditis elegans*

Hayden P. Huggins[1], Jacob S. Subash[1], Hamilton Stoffel[1], Melissa A. Henderson[2,*], Jenna L. Hoffman[1], David S. Buckner[1], Madhu S. Sengupta[3], Peter R. Boag[3], Myon-Hee Lee[4] and Brett D. Keiper[1,‡]

ABSTRACT

Germ cells use both positive and negative mRNA translational control to regulate gene expression that drives their differentiation into gametes. mRNA translational control is mediated by RNA-binding proteins, miRNAs and translation initiation factors. We have uncovered the discrete roles of two translation initiation factor eIF4E isoforms (IFE-1, IFE-3) that bind 7-methylguanosine (m7G) mRNA caps during *Caenorhabditis elegans* germline development. IFE-3 plays important roles in germline sex determination (GSD), where it promotes oocyte cell fate and is dispensable for spermatogenesis. IFE-3 is expressed throughout the germline and localizes to germ granules, but is distinct from IFE-1 and PGL-1, and facilitates oocyte growth and viability. This contrasts with the robust expression in spermatocytes of IFE-1, the isoform that resides within P granules in spermatocytes and oocytes, and promotes late spermatogenesis. Each eIF4E is localized by its cognate eIF4E-binding protein (IFE-1:PGL-1 and IFE-3:IFET-1). IFE-3 and IFET-1 regulate translation of several GSD mRNAs, but not those under control of IFE-1. Distinct mutant phenotypes, *in vivo* localization and differential mRNA translation suggest independent dormant and active periods for each eIF4E isoform in the germline.

KEY WORDS: eIF4E, mRNA translational control, Germline sex determination, 4EBP, Gametogenesis, Polysomes

INTRODUCTION

In germ cells, translation control of mRNAs that leads to new protein synthesis has been shown to be critical for stem cell maintenance, meiotic entry, completion of meiosis and gamete differentiation (Ciosk et al., 2006; Crittenden et al., 1994; Friday and Keiper, 2015). Current models suggest that RNA regulatory networks composed of RNA-binding proteins (RBPs), microRNAs (miRNAs) and translation initiation factors (eIFs) coordinate splicing, transport, storage, translation and degradation of mRNAs by the assembly of messenger ribonucleoprotein (mRNP) complexes. Repression of mRNAs by RBPs and miRNAs has been extensively studied in various developmental systems (Lai et al., 2011; Pillai et al., 2007; Zahr et al., 2018). However, repression is only part of overall translational control. Recent evidence suggests that selective activation of repressed mRNPs by eIF4 factors that recruit them to ribosomes represents a vital step in translational control (Ghosh and Lasko, 2015; Henderson et al., 2009). However, the mechanisms for the transition remain poorly understood. The prevalence of positive mRNA translational control by eIF4 factors in development has only recently begun to be appreciated (Friday and Keiper, 2015; Keiper, 2019).

Translation initiation factors in the eIF4 group are the first to bind mRNAs and recruit them to ribosomes (Rhoads, 1993). Two regulated components are eIF4E and eIF4G, which bind the mRNA 7-methylguanosine 5′-cap (m7G) and act as a scaffold for ribosome association, respectively. The eIF4E:eIF4G interaction is a critical step for mRNA recruitment (Keiper et al., 1999). This node is regulated by eIF4E-binding proteins (4EBPs) that compete with eIF4G for eIF4E interaction and usually inhibit cap-dependent translation (Gingras et al., 2001). We postulate that the eIF4E:eIF4G interaction may actively dissociate 4EBPs from repressed mRNPs and activate translation. To add greater complexity, multiple eIF4E isoforms and 4EBPs are expressed in all invertebrate, vertebrate and plant species studied (Hernández et al., 2005; Joshi et al., 2005; Patrick and Browning, 2012; Wilhelm et al., 2003). Five eIF4E isoforms (IFE-1 through IFE-5) are expressed from the *C. elegans* genome. Individual null strains are mostly viable, and, strikingly, loss of each IFE produces a unique phenotype (Keiper et al., 2000). IFE-1 and IFE-3 are the predominant eIF4Es expressed in the germline (Jankowska-Anyszka et al., 1998). We previously showed that IFE-1 is required for completion of spermatogenesis and, to a lesser extent, oocyte maturation (Friday et al., 2015; Henderson et al., 2009). IFE-1 also binds directly to PGL-1 (Amiri et al., 2001), a core component of P granules that sequesters germ cell mRNAs *in vivo*. PGL-1 is a combined 4EBP RNA-binding protein that is required for normal fertility (Kawasaki et al., 1998). P granules house a large cohort of proteins known to regulate mRNAs post-transcriptionally (Rybarska et al., 2009; Shimada et al., 2006; Voronina et al., 2012). P granules generally localize to nuclear pores and are uniquely poised to regulate the translation and stability of mRNAs exiting the nucleus (Sheth et al., 2010).

In contrast to the role of IFE-1 in the germline, we initially showed that IFE-3 was the only eIF4E essential for embryogenesis in *C. elegans* (Keiper et al., 2000). Mutations in *ife*-3 also disrupt germline sex determination (GSD) (Mangio et al., 2015). We hypothesize that two germ cell eIF4E isoforms (IFE-1, IFE-3) are differentially expressed to promote gamete maturation and sperm/oocyte fate, respectively. The isoforms localize to separable mRNPs that regulate distinct subsets of mRNAs; the identified mRNAs match with their prescribed germ cell functions (Fig. 1A). This study describes the unique germline roles of IFE-3 in the sperm-to-oocyte switch and oocyte growth and contrasts them with the very

[1]Department of Biochemistry and Molecular Biology, Brody School of Medicine at East Carolina University, Greenville, NC 27834, USA. [2]Department of Molecular Sciences, DeBusk College of Osteopathic Medicine, Lincoln Memorial University, Harrogate, TN 37752, USA. [3]Monash Biomedicine Discovery Institute and Department of Biochemistry and Molecular Biology, Monash University, Clayton, VIC 3800, Australia. [4]Department of Internal Medicine, Brody School of Medicine at East Carolina University, Greenville, NC 27834, USA.
*Present address: Rocky Vista University, College of Osteopathic Medicine – Southern Utah, Ivins, UT 84738, USA.

‡Author for correspondence (keiperb@ecu.edu)

P.R.B., 0000-0002-0889-0859; M.-H.L., 0000-0001-9020-2391; B.D.K., 0000-0002-8621-9825

Received 16 August 2019; Accepted 10 February 2020

Journal of Cell Science (2020) 133, jcs237990. doi:10.1242/jcs.237990

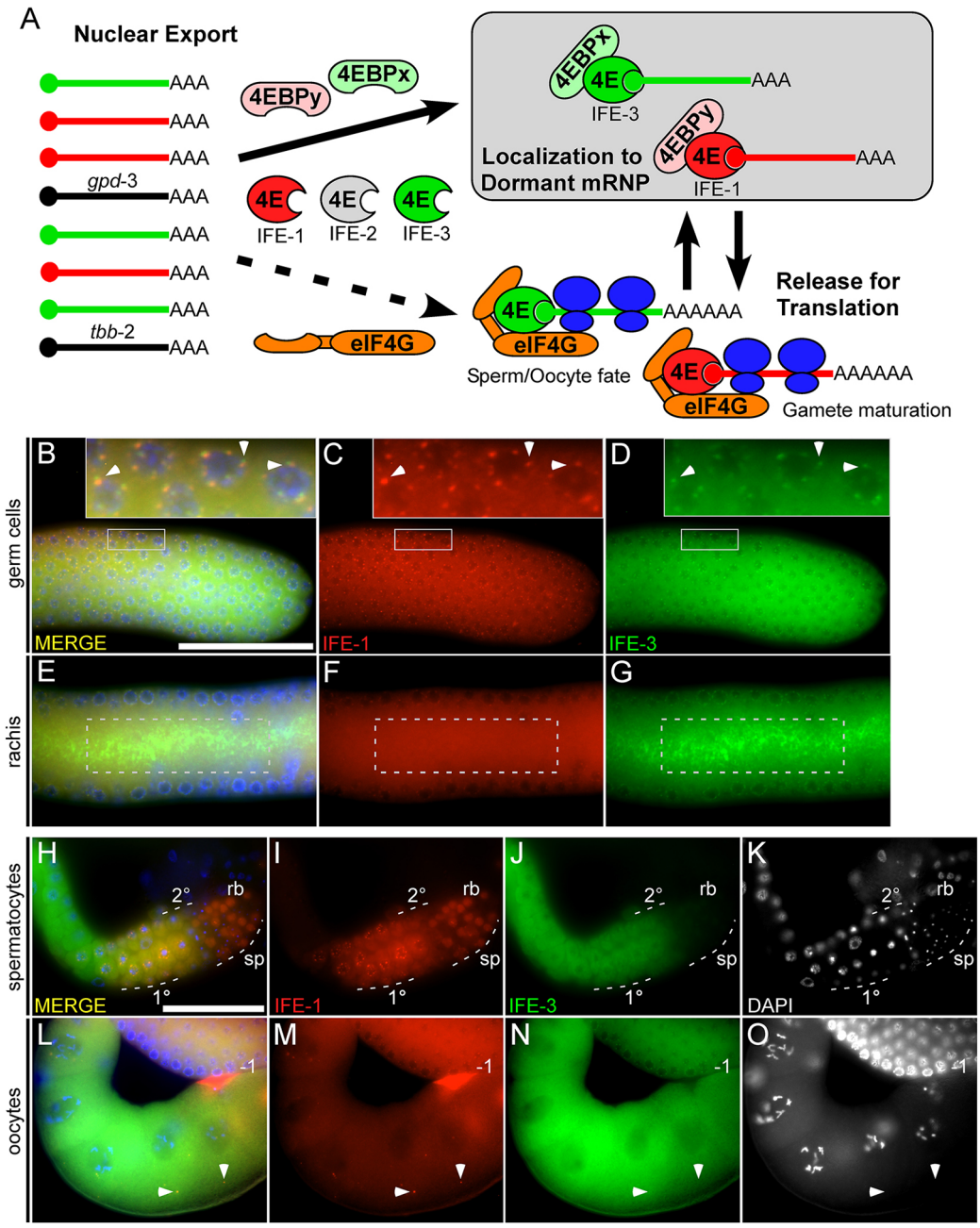

Fig. 1. IFE-1 and IFE-3 localization in germ cells and gametes. (A) Differential translational regulation of mRNAs involved in gamete maturation (red), sperm/oocyte fate (green) and housekeeping mRNAs (black) by germline eIF4E isoforms (IFE-1, -2 and -3). Mutually exclusive binding partners for eIF4Es (4EBPs and eIF4G) regulate mRNA selection by forming a repression-to-activation node after nuclear export. The model, based on this and other studies, is that IFE-1 and IFE-3 use distinct 4EBPs (x and y) for differential spatial and temporal localization in germ granule messenger ribonucleoproteins (mRNPs) that prevent translation of their cargo mRNAs. During germ cell development, each mRNP is remodeled independently. IFE-bound mRNAs are released and recruited by eIF4G to actively translating ribosomal complexes. In this model, direct recruitment by IFE-1 or IFE-3 following nuclear export is unlikely (dashed line arrow). Consequently, the IFEs and their 4EBPs play cooperative roles in both mRNA repression and activation. IFE-2 is a fully soluble germ cell eIF4E not found in granules, and it recruits a different subset of mRNAs (Song et al., 2010). (B–D) IFE-1 (red) and IFE-3 (green) co-expression in distal germ cells shows that they localize to adjacent yet distinct perinuclear foci (insets, arrowheads). Cytosolic IFE-1 and IFE-3 overlap substantially (yellow) throughout distal germ cells. (E–G) Co-expression in the gonad core (dashed line boxes) shows that IFE-1 is soluble and localized diffusely, whereas IFE-3 associates with extensive lattice-like structures. (H–K) Co-expression in spermatocytes shows that IFE-1 is upregulated and becomes enriched in perinuclear foci in primary spermatocytes (1°), but then becomes soluble in secondary spermatocytes (2°). Primary, secondary and spermatid differentiation regions are indicated by the dashed lines. IFE-1 is deposited into residual bodies (rb) after spermatid (sp) budding. IFE-3 does not form perinuclear foci and is diminished during the latter stages of spermatogenesis. (L–O) Co-expression in oocytes shows that IFE-1 forms perinuclear foci that move away from the nucleus (arrowheads) as oocytes approach the spermatheca, whereas IFE-3 is soluble and diffuse. The last oocyte prior to fertilization is indicated by -1. CRISPR/Cas9 fluorescently tagged mKate2::TEV::3xmyc::IFE-1 and GFP::TEV::3xflag::IFE-3 were used to evaluate expression of endogenous genes. Gonads were dissected, fixed and counterstained (DAPI, blue) for nuclear morphology. Scale bars: 50 µm.

different roles of IFE-1. The GSD pathway relies heavily on mRNA translational control (see Fig. 3A). The pathway allows larval animals to transiently produce sperm, then switch to oogenesis. The GLD-1–FOG-2 complex is an upstream factor in GSD that binds the 3′-untranslated region (3′-UTR) of oocyte-promoting *tra*-2 mRNA and represses its translation, which initially promotes larval sperm

Journal of Cell Science (2020) 133, jcs237990. doi:10.1242/jcs.237990

production (Clifford et al., 2000; Goodwin et al., 1993; Jan et al., 1999). The FEM proteins (FEM-1, -2, -3) subsequently promote sperm fate by degrading TRA-1, the transcriptional repressor of the terminal sperm-promoting genes *fog*-1 and *fog*-3 (Starostina et al., 2007). In contrast, oocyte cell fate is promoted by TRA-2 inhibition of FEM-3, which allows TRA-1 to repress *fog*-1 and *fog*-3 (Mehra et al., 1999). *fem*-3-binding factors (FBFs) also promote oocyte cell fate by binding the 3′-UTRs and repressing translation of *fem*-3 and *fog*-1/-3 mRNAs (Thompson et al., 2005; Zhang et al., 1997). Translational control dominates GSD gene expression; however, the means by which opposing fate signal mRNAs, like *tra*-2 and *fem*-3, are coordinated are unclear. How are these signals integrated via negative and positive translational control to allow sperm production in larvae, followed by oogenesis in the adults? Are eIF4E isoforms and their cognate 4EBPs playing a role in this translational control?

Here, we distinguish the roles of IFE-1 and IFE-3, further demonstrating that eIF4E isoforms have different functions during development. We provide evidence that IFE-3 regulates mRNAs in a manner that is distinct from that of IFE-1 to promote oocyte fate and regulate GSD. We also describe the differential expression of IFE-1 and IFE-3 during hermaphrodite germline development using dual-fluorescent CRISPR/Cas9 tagging to show that their expression patterns correlate with their functions. IFE-3 associates with germ granules, but the timing, morphology and developmental pattern is distinct from that of IFE-1 in P granules. IFE-1 and IFE-3 localization depends upon their cognate 4EBPs. Our genetic, biochemical and expression data suggest differential dormant and active periods for IFE-1 and IFE-3 during the progression of germline development.

RESULTS

eIF4E isoforms IFE-1 and IFE-3 localize differently in the germline

Comparing differential eIF4E isoform expression in the germline might provide insight into their divergent functions as well as the distinct phenotypes of each null mutant. To obtain a reliable expression pattern for each isoform, we edited endogenous *ife*-1 and *ife*-3 genes using CRISPR/Cas9 to generate N-terminally fluorescent-tagged mKate2::IFE-1 and GFP::IFE-3, respectively (Dickinson et al., 2015). Strains homozygous for each fusion were fertile and superficially wild type, indicating that each was functional as a translation factor. Both eIF4Es were robustly expressed in the gonad throughout development, but their expression and localization patterns were distinct. Both IFE-1 and IFE-3 localized to perinuclear germ granules, but were also soluble in the cytoplasm of germ cells in the distal gonad (mitotic to early pachytene region; Fig. 1B–D). Our previous study found IFE-1 in embryonic P granules (Amiri et al., 2001). Intriguingly, we observed separate perinuclear localization of IFE-1 and IFE-3 in a strain expressing both IFE fusions (Fig. 1B–D, insets, arrowheads). IFE-1 granules were larger (570±13 nm, n=81) than IFE-3 granules (366±7 nm, n=74) and more numerous. Another striking difference between IFE-1 and IFE-3 was seen in the rachis (gonad core), where IFE-3 associated with lattice-like structures (Fig. 1E–G). IFE-1 did not form similar structures (Fig. 1F). In the distal gonad, the soluble fractions of IFE-1 and IFE-3 were overlapping, unlike their respective granules (Fig. 1B,E, merged images, yellow).

In spermatocytes and oocytes, IFE-1 and IFE-3 localization patterns became even more divergent. Using nuclear morphology to stage spermatocytes (Fig. 1H–K), we observed that IFE-1 was upregulated in primary (1°) spermatocytes, where it formed perinuclear granules, then became largely soluble in secondary (2°) spermatocytes. After spermatid budding, IFE-1 was deposited into residual bodies (Fig. 1I). Conversely, IFE-3 was soluble throughout spermatogenesis and was diminished early in 2° spermatocytes (Fig. 1J). In oocytes, IFE-3 was strongly expressed and fully soluble, whereas IFE-1 formed granules (Fig. 1L–O, arrowheads). Our observations suggest that each eIF4E isoform forms distinct granules in early germ cells, but then each becomes soluble in the respective gametes in which they predominate, IFE-1 in spermatocytes and IFE-3 in oocytes.

IFE-3 promotes the sperm-to-oocyte switch and is important for oocyte development

The *ok191* allele deletes the promoter and first exon of *ife-3* (Fig. 2A). Stably balancing this mutation proved difficult because the *ife-3* locus on the end of chromosome V is a hotspot for meiotic recombination (Mangio et al., 2015). It was therefore necessary to genotype worms from each generation for each experiment using a triple-primer genomic PCR to unambiguously confirm *ok191* (Fig. 2A). Eggs from *ife*-3(+/−) mothers carry sufficient maternal IFE-3 for survival of some *ife*-3(−/−) offspring (Mangio et al., 2015). The escaping *ife*-3(−/−) hermaphrodites developed to adulthood but were sterile at 20°C. Their dissected gonads showed extensive sperm production and lack of oocytes, as evidenced by immunostaining for major sperm protein (MSP) and lack of LIN-41 (oocyte marker) (Fig. 2D). Wild-type hermaphrodite (Fig. 2B) and male (Fig. 2C) germlines are shown for comparison. These data demonstrate that *ife*-3 mutant hermaphrodites have masculinized germlines (Mog) and fail to produce oocytes at 20°C. Surprisingly, at elevated temperatures (25°C), at least 21% of *ife*-3(−/−) hermaphrodites were able to initiate oogenesis (Fig. 2E). Oocytes were evident in the proximal gonad by their expression of LIN-41 but did not grow normally. These results indicate that IFE-3 has roles in oocyte development beyond the sperm-to-oocyte switch. This phenotype differs strikingly from that of *ife*-1(*bn127*) worms, which arrests late spermatocyte differentiation and maturing oocytes (Friday et al., 2015; Henderson et al., 2009). Temperature obviously plays a role in the sterility caused by both *ife*-1 and *ife*-3 mutations. However, the sterility seen in *ife*-3 worms is alleviated at elevated temperatures, whereas the sterility seen in *ife*-1 worms is exacerbated by it.

We determined the prevalence of the *ife*-3 sterility at 20°C and 25°C. No heterozygous *ife*-3(+/−) hermaphrodites were sterile at 20° C (n=61) or 25°C (n=49) (Fig. 2F). However, 100% of *ife*-3(−/−) hermaphrodites were sterile (n=60) at 20°C, due to the Mog phenotype. Interestingly, only 79% of *ife*-3(−/−) hermaphrodites were sterile (n=62) at 25°C, indicating a ∼20% rescue of oocyte fate (Fig. 2F). The *ife*-3(−/−) mutants had smaller brood sizes (84±7, n=4) compared to wild-type animals (221±10, n=3) at 25°C (data not shown), and the embryos from *ife*-3(−/−) mothers never hatched (Fig. 2F). This observation supports our previous finding using *ife*-3(RNAi), which showed substantial embryonic lethality (Keiper et al., 2000). Curiously, the distal gonads of *ife*-3(−/−) hermaphrodites were occasionally bifurcated at 20°C (8%, n=60) and at 25°C (5%, n=62) (data not shown). These phenotypes are unique to *ife*-3 among the eIF4E isoforms, since neither the Mog phenotype nor the aberrant gonad morphology was ever observed in *ife*-1(*bn127*), *ife*-2(*ok306*), *ife*-4(*ok320*) or *ife*-5(*ok1934*) animals (Amiri et al., 2001; Dinkova et al., 2005; Henderson et al., 2009; Song et al., 2010). Lastly, we addressed whether IFE-3 was required for male-derived sperm to fertilize oocytes upon mating with *fog*-2(*q71*) females, as was previously found for IFE-1 (Henderson et al., 2009). Soaking males in SYTO17 labels their sperm for detection after mating

Journal of Cell Science (2020) 133, jcs237990. doi:10.1242/jcs.237990

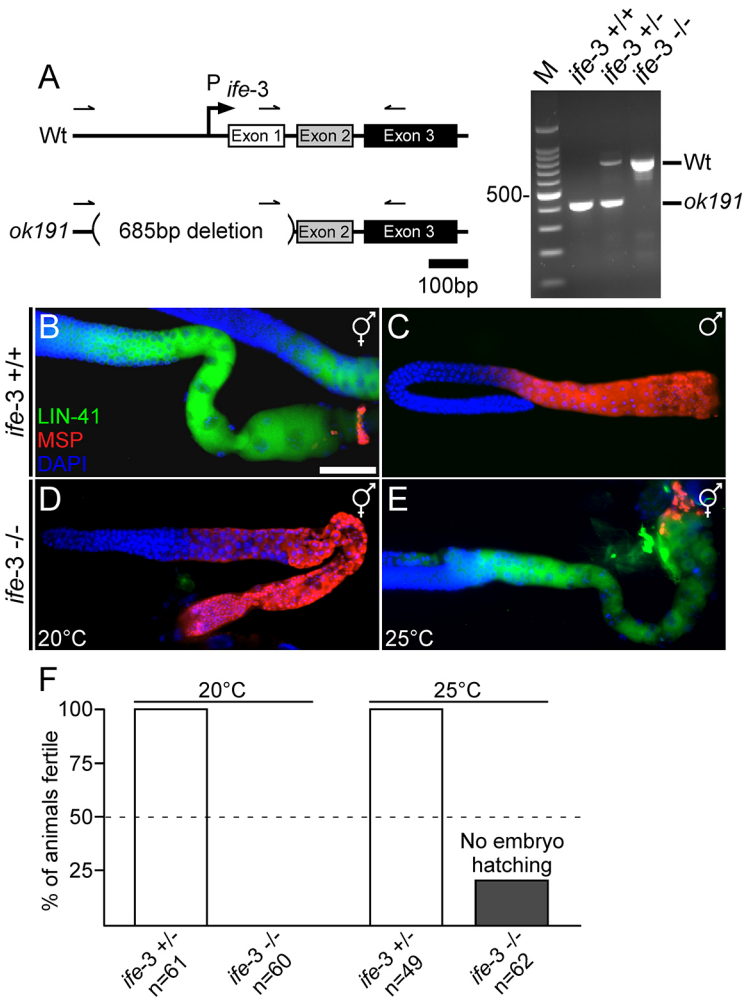

Fig. 2. Characterization of *ife*-3(*ok191*) mutants. (A) Schematic of *ife*-3 on chromosome V (left). The *ok191* deletion removes the promoter and exon 1. The gel (right) shows whole-worm genomic PCR at the *ife*-3 locus from wild-type (+/+), heterozygous (+/–) and homozygous (–/–) animals. (B) Wild-type hermaphrodite gonad showing sperm in the spermatheca stained for major sperm protein (MSP; red), and oocytes, showing LIN-41 expression (green). (C) Wild-type male gonad showing only MSP-stained sperm and no LIN-41. (D) *ife*-3(–/–) hermaphrodite gonad showing masculinization phenotype (Mog) at 20°C, as indicated by overabundance of MSP-stained sperm throughout the gonad, and complete lack of LIN-41-expressing oocytes. (E) *ife*-3(–/–) hermaphrodite gonad showing both MSP-stained sperm and small LIN-41-expressing oocytes at 25°C. (F) Fertility and embryonic viability in *ife*-3(+/–) and *ife*-3(–/–) mothers at both 20°C and 25°C. Genotype of each individual was confirmed by genomic PCR. Germlines shown (B–E) carry *lin*-41(*tn1541*[*gfp*::*tev*::*s*::*lin*-41])I to visualize oocytes and were dissected, fixed, stained with anti-MSP antibody and counterstained (DAPI, blue). Scale bar: 50 µm.

(Fig. S2A–D). Although *ife*-3(−/−) males had somewhat decreased mating efficiency at 25°C, their sperm were able to fertilize eggs in 100% of *fog*-2(*q71*) females at both 20°C and 25°C (Fig. S2B,E). Males lacking IFE-1 produce very few sperm at 20°C (Henderson et al., 2009), but still fertilized eggs in 100% of *fog*-2(*q71*) females. By contrast, *ife*-1(−/−) males produced no sperm at 25°C, resulting in no fertilization events (Fig. S2D,E). These data establish that IFE-3 is dispensable for producing functional sperm regardless of temperature, in stark contrast to IFE-1, which is required for spermatogenesis at 25°C.

ife-3 promotes oocyte fate together with *fbf* genes in the GSD pathway

Many mutations that alter the sexual fates of germ cells have been identified in *C. elegans* (Barton and Kimble, 1990; Schedl and Kimble, 1988). Most of the corresponding GSD genes encode RBPs or mRNAs within a translational control network that culminates in the conditional synthesis of FOG-1/-3, which drives sperm fate (Fig. 3A). To understand where *ife*-3 might function in this network, we conducted epistatic analyses with mutations in components of the GSD pathway in conjunction with IFE-3 depletion. We chose to use *ife*-3(RNAi) for these experiments due to the embryonic lethality of *ife*-3(*ok191*) and the instability of the balanced mutation, both of which complicate the derivation of double mutant strains. Following *ife*-3(RNAi) treatment, 22% (*n*=157) of wild-type hermaphrodites failed to produce oocytes and developed the Mog phenotype, as evident by extensive MSP staining and apparent lack of oocytes (Fig. 3B,D). The penetrance of *ife*-3(RNAi)-induced sterility is lower than that of the null allele (22% vs 79% at 25°C, respectively). By comparison, 100% (*n*=129) of control(RNAi)-treated wild-type hermaphrodites showed both sperm and oocytes (Fig. 3B,C). To rule out the possibility of weak *ife*-3(RNAi) efficacy, we also performed *ife*-3(RNAi) in an RNA interference (RNAi)-sensitized strain *eri*-1(*mg366*), but obtained similar frequencies of Mog phenotype (20%, *n*=86; Fig. 3B).

To place *ife*-3 within the GSD pathway, we looked for reversion of feminizing mutations or enhancement of Mog phenotype by *ife*-3(RNAi). The *fog*-2(*q71*) mutation results in feminized hermaphrodite germlines (Fog phenotype) that never produce sperm (Schedl and Kimble, 1988) and is an upstream factor in the GSD pathway (Fig. 3A). Consistent with this, Fog gonads were observed in 100% (*n*=117) of control(RNAi)-treated *fog*-2(*q71*) hermaphrodites, as evident by the absence of MSP staining and the presence of large stacked oocytes (Fig. 3B,E). By contrast, 23% (*n*=127) of *ife*-3(RNAi)-treated *fog*-2(*q71*) hermaphrodite gonads developed as Mog, showing extensive MSP staining and no oocytes (Fig. 3B,F). IFE-3 depletion was thus able to revert the *fog*-2(*q71*) feminizing mutation at a similar frequency to wild-type animals, indicating that *ife*-3 promotes oocyte fate downstream of *fog*-2. Another feminizing mutation, *fem*-3(*e2006*), also causes hermaphrodites to develop Fog at 25°C but not 20°C (Hodgkin, 1986). As expected, none of the control(RNAi)-treated *fem*-3(*e2006*)

Journal of Cell Science (2020) 133, jcs237990. doi:10.1242/jcs.237990

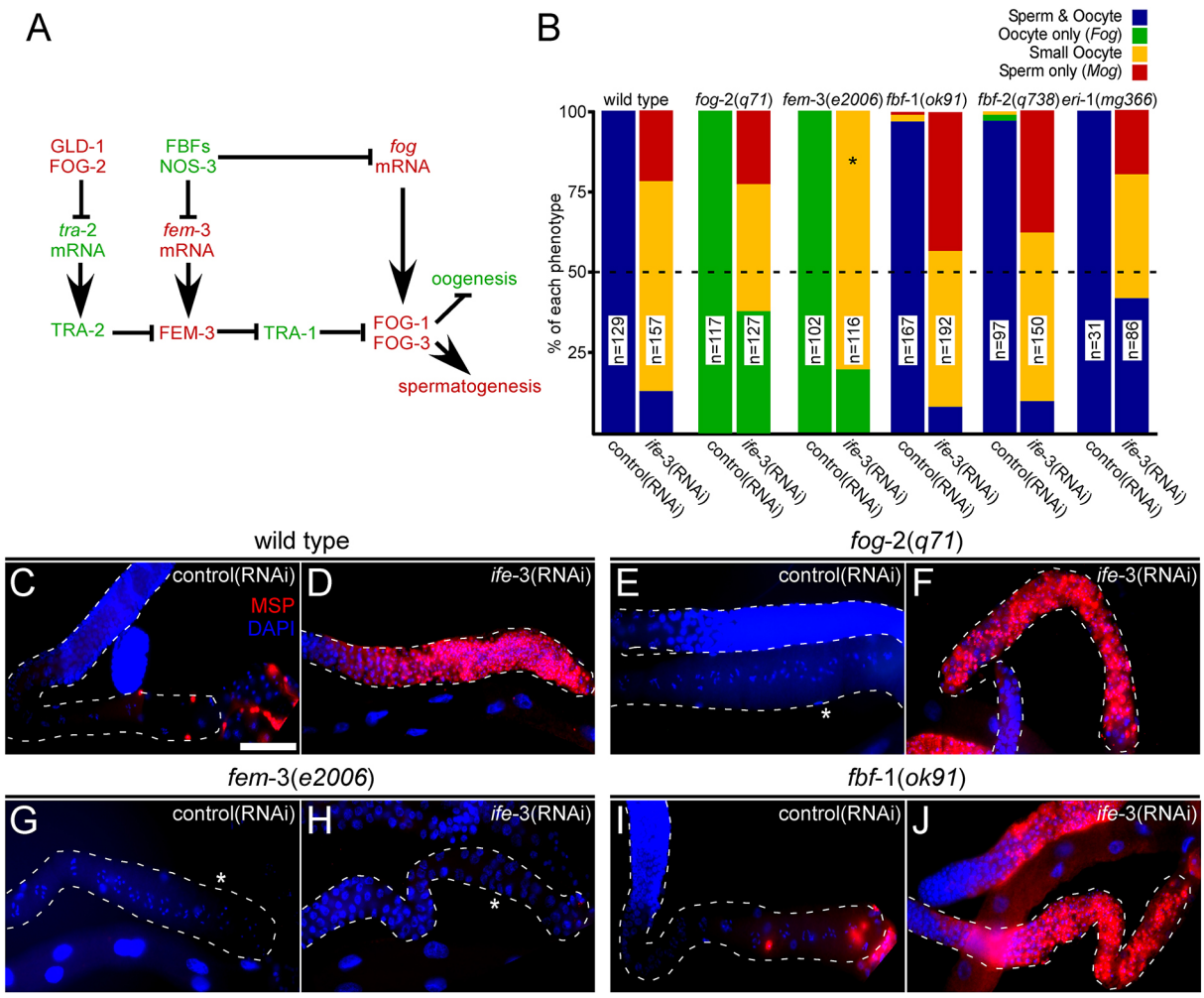

Fig. 3. Epistatic analysis of *ife*-3 and other regulators of GSD. (A) Germline sex determination (GSD) in *C. elegans* is a series of positive and negative genetic switches that rely on mRNA translational control. Factors that drive sperm fate (red) or oocyte fate (green) are shown. (B) Epistatic outcomes from *ife*-3(RNAi) in mutant backgrounds depicted in a bar graph that shows the distributions of phenotypes for each group. (C) Control(RNAi)-treated wild-type hermaphrodite gonad showing sperm (MSP, red) and oocytes, as identified by nuclear morphology (DAPI, blue). (D) *ife*-3(RNAi)-treated wild-type hermaphrodite gonad showing masculinization phenotype (Mog) as indicated by an overabundance of sperm and lack of oocytes. (E) Control(RNAi)-treated *fog*-2(*q71*) gonad showing feminization phenotype (Fog), as indicated by lack of MSP-stained sperm and presence of stacked oocytes. (F) *ife*-3(RNAi)-treated *fog*-2(*q71*) gonad showing Mog phenotype, demonstrating reversion of *fog*-2(*q71*)-induced feminization. (G) Control(RNAi)-treated *fem*-3(*e2006*) gonad showing Fog phenotype. (H) *ife*-3(RNAi)-treated *fem*-3(*e2006*) gonad showing Fog phenotype with small germ cells. No sperm were ever observed in *fem*-3(*e2006*) worms (B), demonstrating failure to revert the feminization phenotype (asterisk). The resulting small germ cells were later found to be LIN-41-expressing oocytes (Fig. 4A). (I) Control(RNAi)-treated *fbf*-1(*ok91*) gonad showing sperm and oocytes. (J) *ife*-3(RNAi)-treated *fbf*-1(*ok91*) gonad showing Mog phenotype. *fbf*-1(*ok91*) mutants treated with *ife*-3(RNAi) displayed enhanced penetrance of Mog phenotype relative to wild-type animals. Germlines of the indicated genotype were dissected, fixed, stained for MSP to visualize sperm and counterstained (DAPI, blue). Gonads are outlined (dashed lines) for clarity. Fog phenotype is denoted by asterisks. Scale bar: 50 µm.

hermaphrodites were Mog at 25°C (0%, *n*=102; Fig. 3B,G). None of the *ife*-3(RNAi)-treated worms (0%, *n*=116) developed as Mog, as shown by the lack of MSP staining (Fig. 3B,H). IFE-3 depletion was therefore unable to revert the *fem*-3(*e2006*) feminizing mutation, indicating that *ife*-3 promotes oocyte fate at a step genetically upstream or at *fem*-3, consistent with the findings of Mangio et al. (2015). FBF-1 and FBF-2 (*fem*-3-binding factors) are homologous RBPs that repress translation of *fem*-3 and *fog*-1/-3 mRNAs to promote oocyte cell fate (Thompson et al., 2005; Zhang et al., 1997). *fbf*-1(*ok91*) mutants are slightly masculinized (1% Mog), and *fbf*-2(*q738*) mutants are slightly feminized (1% Fog), for reasons that remain unclear (Lamont et al., 2004; Yoon et al., 2017). *ife*-3(RNAi) masculinized 43% (*n*=192) of *fbf*-1(*ok91*) hermaphrodites (Fig. 3B,J), whereas only 1% displayed Mog phenotype upon control(RNAi) (Fig. 3B,I). Therefore, IFE-3 depletion enhanced Mog penetrance 2-fold in *fbf*-1 mutants relative to *ife*-3(RNAi)-treated wild-type animals. Similarly, enhanced Mog penetrance was seen in *fbf*-2(*q738*) hermaphrodites (Fig. 3B). These data show that *ife*-3 and *fbf* genes act synergistically to promote oocyte fate, suggesting that IFE-3 works with FBFs in translational control.

A substantial number of *ife*-3(RNAi) hermaphrodites were not Mog, but developed small, stunted oocytes that failed to develop normally (Fig. 3B,H). This was first observed in some *ife*-3(−/−) null worms grown at 25°C (Fig. 2E) but was more consistent upon *ife*-3(RNAi). Small oocytes were observed in 39–80% of IFE-3-depleted worms, depending on the genetic background, and was most prevalent when masculinization could not be achieved (Fig. 3B,H; e.g. *fem*-3). Small cells were negative for MSP staining and were confirmed to be oocytes by LIN-41 expression (Fig. 4A). Staining with 4′,6-diamidino-2-phenylindole (DAPI)

Journal of Cell Science (2020) 133, jcs237990. doi:10.1242/jcs.237990

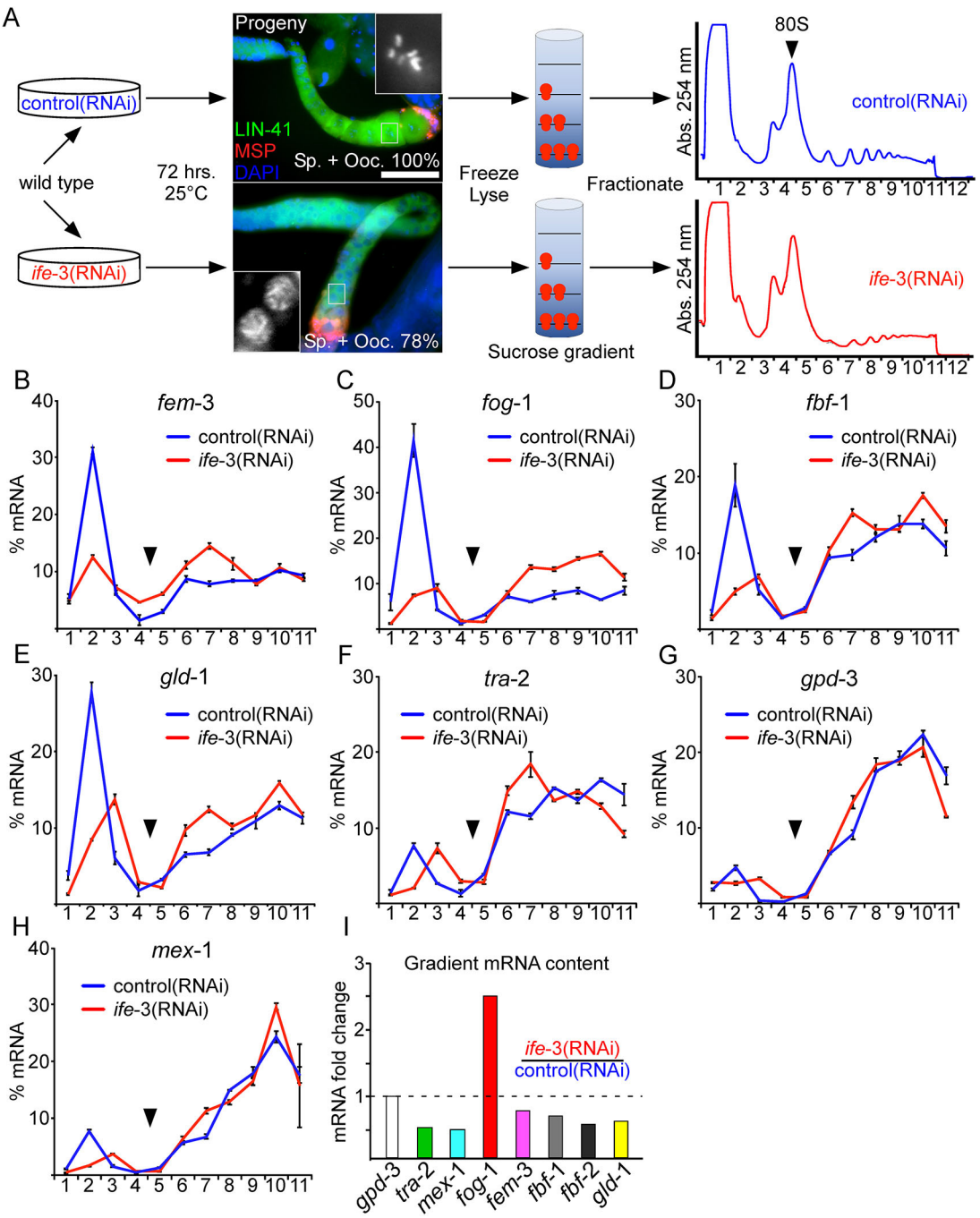

Fig. 4. Translational efficiency of GSD mRNAs is altered by IFE-3 depletion. (A) Schematic of the experimental design for high-resolution polysome analysis. Wild-type animals were grown on control(RNAi) (blue) or *ife*-3(RNAi) (red). Micrographs depict representative phenotypes of control(RNAi) or *ife*-3(RNAi) worms. As before, IFE-3 depletion resulted in a minority (22%) of Mog animals; the majority (78%) remained oogenetic. Absorbance (A_{254}) profiles for gradient fractionation of extracts from control(RNAi) (blue) and *ife*-3(RNAi)-treated (red) worms depict the polysome content. The highest resolved peak is the monosome (80S position is indicated by arrowhead) and each peak to the right represents the addition of one ribosome (polysomes). (B–H) Individual graphs depict normalized mRNA content across the gradient by qRT-PCR for *fem*-3 (B), *fog*-1 (C), *fbf*-1 (D), *gld*-1 (E), *tra*-2 (F), *gpd*-3 (G) and *mex*-1 (H) mRNAs. Normalization by total RNA content across the gradient corrects for slight differences in polysome yield, allowing direct comparison of the partitioning of each mRNA. Error bars indicate the s.d. of triplicate qRT-PCR measurements. Similar profiles were obtained for *fem*-3, *fog*-1 and *gpd*-3 mRNAs in two to three independent experiments. (I) Relative mRNA abundance in each gradient (normalized to *gpd*-3) shows that in *ife*-3(RNAi)-treated animals, *fog*-1 is increased 2.5-fold, while all other mRNAs assayed (*tra*-2, *mex*-1, *fem*-3, *fbf*-1, *fbf*-2 and *gld*-1) were decreased by 25–50% compared to control(RNAi)-treated animals. Germlines shown (A) carry *lin*-41(*tn1541*[*gfp*::*tev*::*s*::*lin*-41])I to visualize oocytes and were dissected, fixed, stained for MSP to visualize sperm and counterstained (DAPI, blue). Scale bar: 50 µm.

confirmed aberrant nuclear morphology, indicating defects in meiosis (Fig. 4A, insets). Both the RNAi and null mutation phenotypes indicate that IFE-3 must have roles beyond GSD in oocyte growth and completion of meiosis.

IFE-3 regulates the translation of some GSD mRNAs

Because eIF4E isoforms bind to mRNA caps and catalyze translation initiation, we postulated that IFE-3 loss might adversely affect the translation of GSD pathway mRNAs. We

Journal of Cell Science (2020) 133, jcs237990. doi:10.1242/jcs.237990

directly analyzed the translational efficiency of several GSD mRNAs in control and *ife*-3(RNAi)-treated wild-type animals using high-resolution polysome profiling (King and Gerber, 2014). Our previous studies used identical methodology to analyze mRNAs that respond to IFE-1, IFE-2 and IFE-4 deficiencies *in vivo* (Dinkova et al., 2005; Friday et al., 2015; Henderson et al., 2009; Song et al., 2010). Each IFE isoform previously investigated positively regulates a unique subset of mRNAs. Large scale *ife*-3(RNAi) over a single generation provided sufficient material for sucrose fractionation of whole worm populations and allowed mRNAs to be resolved by their polysome loading (Fig. 4A). RNAi treatment induced Mog phenotype in a minority of the worms, whereas most (78%; Fig. 4A) produced primarily oocytes. IFE-3 depletion was confirmed under these conditions (Fig. S1A–C). Overall polysome content relative to 80S was modestly decreased by *ife*-3(RNAi), indicating that IFE-3 depletion does not dramatically alter bulk protein synthesis. Individual mRNAs were quantified across gradient fractions (Fig. 4B–H). The translation of *fem*-3, *fog*-1, *fbf*-1, *gld*-1 and *tra*-2 were altered upon *ife*-3(RNAi) treatment when compared to control(RNAi)-treated animals (Fig. 4B–F). Unexpectedly, several GSD mRNAs translated more efficiently after IFE-3 depletion. A substantial fraction of non-translating *fem*-3 mRNA (fractions 1–4) in control(RNAi) worms became shifted into light polysomes (fractions 5–8) upon *ife*-3(RNAi), indicating that IFE-3 deficiency allowed for more efficient initiation of *fem*-3 mRNA (Fig. 4B). Strikingly, the bulk of *fog*-1 mRNA also shifted from non-translating fractions into both light and heavy polysomes upon IFE-3 depletion (Fig. 4C). Polysomal loading of *fog*-1 mRNA was therefore greatly enhanced, particularly in the heavy fractions (9–11), where many ribosomes translate simultaneously. The synthetic output of FOG-1 is expected to be higher and might contribute to the Mog phenotype observed (Fig. 3). *fbf*-1 and *gld*-1 mRNAs experienced more modest increases in translational efficiency after IFE-3 depletion. For these, some non-translating mRNA (fractions 1–4) appeared to shift to light and heavy polysomes (Fig. 4D,E). Given the amount of *fbf*-1 and *gld*-1 mRNAs already translating in control(RNAi) worms, the output of these proteins may not be substantially changed. *tra*-2 mRNA was less efficiently translated after IFE-3 depletion, as shown by a shift to light polysomes (Fig. 4F, fractions 5–8) from heavy polysomes (Fig. 4F, fractions 9–11). The effect is modest, but a positive dependence of *tra*-2 translation on IFE-3 is consistent with the role of IFE-3 in promoting oocyte fate. Importantly, the translational efficiency of some mRNAs was unchanged upon *ife*-3(RNAi), including the housekeeping mRNAs GAPDH (*gpd*-3; Fig. 4G) and β-tubulin (*tbb*-2; not shown). Neither show preferential dependence on any single IFE (Dinkova et al., 2005; Friday et al., 2015; Song et al., 2010). More strikingly, *mex*-1 mRNA translational efficiency was also unchanged (Fig. 4H). We previously showed *mex*-1 mRNA translation to be strongly IFE-1 dependent (Henderson et al., 2009). By summing mRNA content across gradients, relative to *gpd*-3 mRNA, we found that, with the exception of *fog*-1, all germline mRNAs assayed were decreased ∼25–50% in *ife*-3(RNAi)-treated animals (Fig. 4I). This is consistent with *ife*-3(RNAi)-treated germlines being smaller than their control(RNAi)-treated counterparts (Fig. 4A). Therefore, changes in the translational efficiency seen were not due to alterations in the abundance of the mRNAs. These data suggest that IFE-3 is involved in the translation of several GSD mRNAs, but not housekeeping mRNAs, nor those regulated by IFE-1. IFE-3 acts to repress *fem*-3, *fog*-1, *fbf*-1 and *gld*-1 mRNA translation, and possibly enhance *tra*-2 mRNA translation. While a negative translational role for an initiation factor was unexpected, it is interesting that the mRNAs repressed by IFE-3 are also well-defined FBF targets (see Discussion and Kershner and Kimble, 2010).

IFE-3 regulates the steady-state levels of some GSD mRNAs

Of the mRNAs assayed translationally, only *fog*-1 mRNA levels appeared to increase upon *ife*-3(RNAi). We wondered whether these changes were due to IFE-3 loss or the 22% of Mog animals in the population (Figs 3B and 4A,I). It is possible that the levels of sperm-promoting mRNAs (*fem*-3 or *fog*-1) increase following complete loss of IFE-3. Indeed, some studies suggest that steady-state *fem*-3 mRNA levels increase in certain Mog backgrounds (Zanin et al., 2010), while others demonstrated that *fog*-1 transcription is enhanced under conditions that favor spermatogenesis (Luitjens et al., 2000). We determined the relative *fem*-3 and *fog*-1 steady-state mRNAs levels relative to *tbb*-2 mRNA in *ife*-3(−/−) L4 hermaphrodites and compared them to wild-type animals. Early and late L4 hermaphrodites were analyzed in order to compare equivalent spermatogenic germlines (avoiding comparison of disparate oogenetic and Mog germlines). We found no statistically significant difference (P=0.328) in *fem*-3 mRNA levels between *ife*-3(−/−) and wild-type early L4 hermaphrodites (Fig. 5A). However, a large and statistically significant increase (9-fold; P=0.007) in

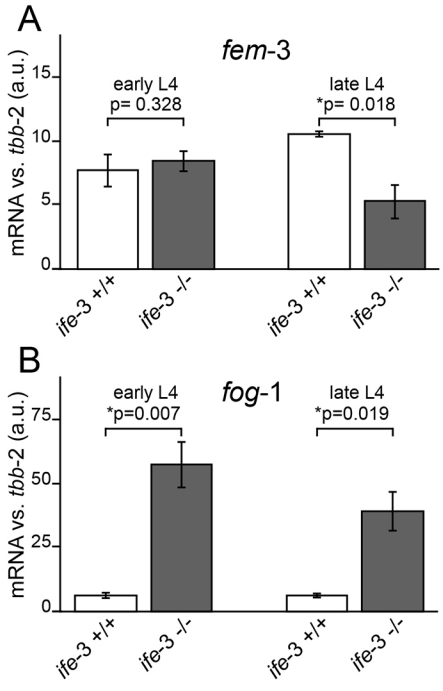

Fig. 5. Steady-state levels of *fem*-3 and *fog*-1 mRNAs in *ife*-3(*ok191*) hermaphrodites. (A) Relative *fem*-3 mRNA expression in early L4 hermaphrodites shows no statistically significant change (P=0.328) between *ife*-3(−/−) (gray) and wild-type (white) animals. Relative *fem*-3 mRNA expression in older L4 hermaphrodites shows a statistically significant (P=0.018) 2-fold decrease in *ife*-3(−/−) animals. (B) Relative *fog*-1 mRNA expression in early L4 hermaphrodites shows a 9-fold increase (P=0.007) in *ife*-3(−/−) animals (gray) compared to wild type (white). Relative *fog*-1 mRNA expression in older L4 hermaphrodites shows a similar 6-fold increase (P=0.019) in *ife*-3(−/−) animals. Animals were synchronized and staging of L4 larvae was confirmed via vulva morphology. Triplicate qRT-PCR measurements from three independent biological replicates are shown, with error bars indicating s.d. Quantifications were normalized to tubulin (*tbb*-2) mRNA. Student's *t*-test was used to determine statistical significance between wild-type and mutant animals (*P<0.05). a.u., arbitrary unit.

Journal of Cell Science (2020) 133, jcs237990. doi:10.1242/jcs.237990

fog-1 mRNA levels was found in early L4 *ife*-3(−/−) hermaphrodites compared to wild-type animals (Fig. 5B). We also examined late L4 worms to determine if the changes in *fem*-3 and *fog*-1 mRNA levels were maintained through the sperm-to-oocyte switch, since these animals are expected to have initiated oogenesis. The *fem*-3 mRNA levels were decreased by half in *ife*-3(−/−) worms relative to wild type (P=0.018; Fig. 5A), again consistent with having smaller germlines. However, *fog*-1 mRNA levels remained 6-fold higher in *ife*-3(−/−) worms (P=0.019; Fig. 5B). These data suggest that IFE-3 loss resulted in enhanced transcription/stabilization of *fog*-1 mRNA even prior to the sperm-to-oocyte switch; *fem*-3 mRNA levels do not change prior to the sperm-to-oocyte switch, but drop at later stages, likely due to the size of the gonad relative to the soma.

IFE-3 localizes to perinuclear granules adjacent to IFE-1: PGL-1 granules

We confirmed IFE-1 residence in P granules of distal germ cells by colocalization with a PGL-1::GFP CRISPR fusion. We observed a high degree of overlap for IFE-1 and PGL-1 in germ cells (Fig. 6A–C, insets, arrowheads). IFE-1 expression was notably upregulated in 1° spermatocytes from L4 hermaphrodites, where it was enriched in PGL-1 granules (Fig. 6D–F). Importantly, IFE-1 left PGL-1 granules and became soluble when PGL-1 disappeared from 2° spermatocytes (Fig. 6E, dashed line). It is likely that PGL-1 stabilizes IFE-1 in P granules. Similarly, IFE-1 was present in PGL-1 granules that moved toward the cortex as oocytes approached the spermatheca (Fig. 6G–I, arrowheads). These data link IFE-1 tightly to PGL-1 in P granule dynamics. Furthermore, IFE-1 becomes completely soluble during late spermatogenesis, at a time and place during development that matches the *ife*-1(*bn127*) phenotype (Amiri et al., 2001; Henderson et al., 2009). We wondered whether the perinuclear IFE-3 granules in distal germ cells also colocalized with PGL-1, considering that IFE-1 and IFE-3 granules appeared distinct (Fig. 1B–D). Unlike IFE-1 foci, the IFE-3 foci were adjacent but clearly separate from PGL-1 (Fig. 6A vs J, insets, arrowheads). We often observed multiple IFE-3 foci decorating a singular PGL-1 granule (Fig. 6J–L, insets, top arrowheads). This was never observed for IFE-1. Also, in contrast

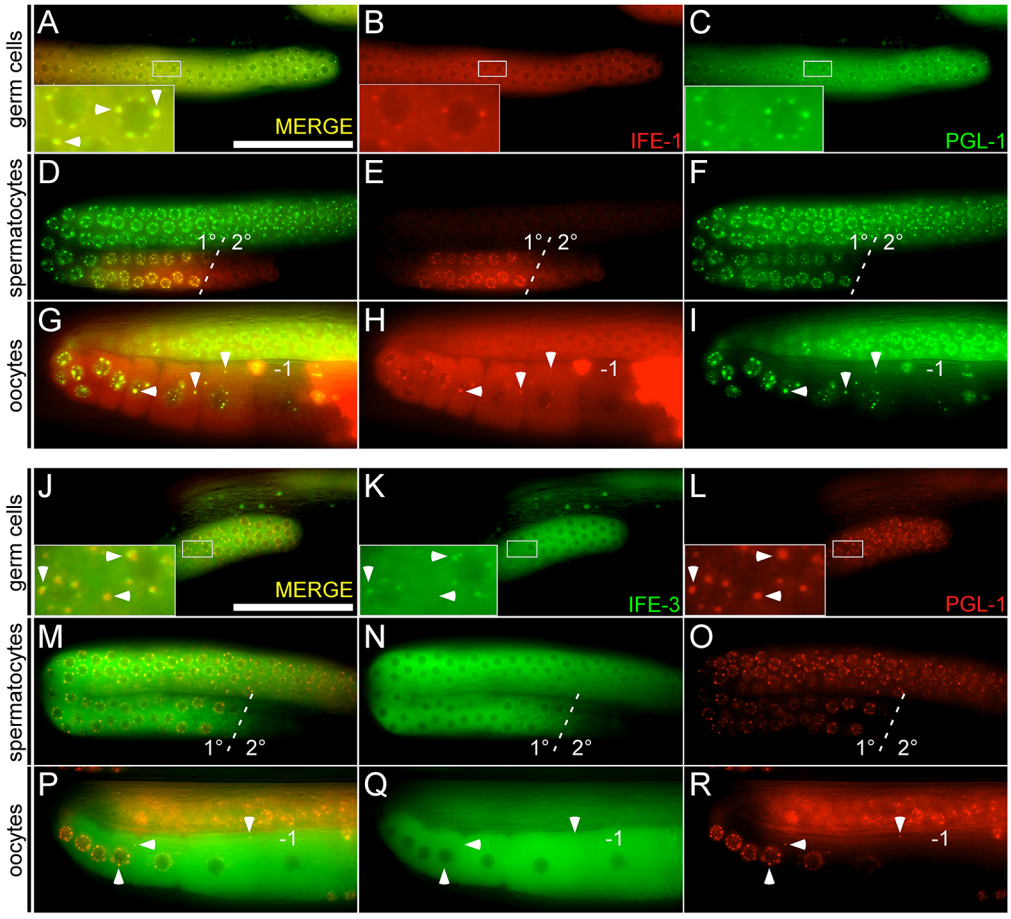

Fig. 6. IFE-1 and IFE-3 localization in the germline relative to PGL-1. (A–C) IFE-1 (red) and PGL-1 (green) co-expression in distal germ cells shows that IFE-1 localizes to P granules (insets, arrowheads) with perfect overlap. (D–F) Co-expression in an L4 hermaphrodite gonad shows that IFE-1 is upregulated during spermatogenesis and becomes enriched in PGL-1 granules in primary spermatocytes (1°). Upon PGL-1 disappearance from secondary spermatocytes (2°), IFE-1 is lost from granules and becomes soluble. (G–I) Co-expression in an adult hermaphrodite gonad shows that IFE-1 localizes to PGL-1 granules that move toward the cortex as oocytes approach the spermatheca (arrowheads). There is also substantial soluble IFE-1 in oocytes. (J–L) IFE-3 (green) and PGL-1 (red) co-expression in distal germ cells shows that IFE-3 perinuclear granules are adjacent yet distinct from PGL-1 granules (insets, arrowheads). Multiple IFE-3 foci surrounding a singular PGL-1 focus were frequently observed (J–L, top arrowhead). (M–O) Co-expression in an L4 hermaphrodite shows that IFE-3 expression is relatively constant and soluble throughout spermatogenesis, not enriched in granules. (P–R) Co-expression in an adult hermaphrodite gonad shows that IFE-3 is completely soluble in oocytes, not localized to PGL-1 granules (arrowheads). The boundary between primary and secondary spermatocytes is indicated by a dashed line. The last oocyte prior to fertilization is indicated by -1. CRISPR/Cas9 fluorescently tagged mKate2::TEV::3xmyc::IFE-1 and GFP::TEV::3xflag::IFE-3 were used to evaluate expression. CRISPR-tagged PGL-1 of the reciprocal color was used to track expression of endogenous PGL-1. Gonads were imaged in immobilized live animals. Scale bars: 50 µm.

Journal of Cell Science (2020) 133, jcs237990. doi:10.1242/jcs.237990

to IFE-1, IFE-3 expression levels were not obviously upregulated during spermatogenesis but remained constant (Fig. 6N vs E) and largely soluble rather than enriched in granules (Fig. 6M–O). IFE-3 was strongly expressed in large oocytes, where it also appeared to be completely soluble (Fig. 6P–R, arrowheads). Considering that oocyte growth and embryogenesis have a greater requirement for IFE-3 (Fig. 2E) than IFE-1 (Henderson et al., 2009), soluble IFE-3 likely participates in protein-synthetic events that contribute to both. In healthy oocytes and spermatocytes, IFE-1 localization is tightly linked to its cognate 4EBP, PGL-1, whereas IFE-3 localization is not. Finally, the major soluble eIF4E isoform in spermatocytes is IFE-1, whereas IFE-3 is the abundant soluble isoform in oocytes.

IFET-1 controls the localization of IFE-3 and together they repress GSD mRNA translation

IFET-1 is the worm ortholog of mammalian eIF4E transporter protein, which facilitates nucleoplasmic shuttling of eIF4E (Dostie et al., 2000). IFE-3 and IFET-1 are found in OMA-1 mRNP complexes *in vivo* (Spike et al., 2014). Others have shown that recombinant IFET-1 is able to bind each of the recombinant IFEs except IFE-4 (Li et al., 2009). Although IFET-1 shows the potential to bind several IFEs *in vitro,* isolation of native mRNP complexes provides evidence of the IFE-3:IFET-1 interaction only (Spike et al., 2014; M.S.S. and P.R.B., unpublished). Thus, IFET-1 is thought to represent a cognate 4EBP for IFE-3. We hypothesized that loss of IFET-1 would disrupt IFE-3 localization, while having no effect on IFE-1 localization. We depleted IFET-1 by RNAi and re-examined localization patterns. IFET-1 depletion was confirmed by loss of IFET-1::GFP expression (Fig. S1D–F). In our hands, *ifet*-1(RNAi)-treated animals had similar phenotypes (data not shown) to those reported for *ifet*-1(*tm2944*), including poor oocyte growth, occasional Mog and bifurcated distal gonads (Sengupta et al., 2013). Importantly, these are similar phenotypes to those of *ife*-3(*ok191*) (Fig. 2). Depletion of IFET-1 disrupted IFE-3 localization to perinuclear granules in distal germ cells (Fig. 7A vs B, insets, arrowheads) without disrupting perinuclear PGL-1 granules (Fig. S3A vs B, insets). Likewise, *ifet*-1(RNAi) prevented IFE-3 localization to lattice-like structures in the gonad core (Fig. 7C vs D, insets). However, the inverse was not the case. IFET-1 localization to perinuclear granules (Fig. 7E vs F) and lattice-like structures in the rachis (Fig. 7G vs H) were unaffected by *ife*-3(RNAi). These data provide evidence of hierarchical binding of IFE-3 to IFET-1, similar to that found for IFE-1:PGL-1 (Amiri et al., 2001). Therefore, localization of IFE-3 to perinuclear granules and rachis structures depends on its cognate 4EBP, IFET-1. IFE-3 and IFET-1 expression patterns were very similar throughout the germline (Fig. 7A,C vs E,G). In contrast to IFE-3, IFE-1 localization to perinuclear PGL-1 granules was maintained following depletion of IFET-1 (Fig. 7I,J vs 7A,B and Fig. S3E,F, insets, arrowheads). However, upon *ifet*-1(RNAi), aberrant aggregates formed in the rachis that contained IFE-1 and PGL-1 (Fig. 7K vs 7L and Fig. S3H, insets). These aggregates appeared quite dissimilar to IFE-3 or IFET-1 lattice-like structures and are likely unrelated. Similar PGL-1 mislocalization was observed by others in *ifet*-1(*tm2944*) germlines (Sengupta et al., 2013), which likely causes the IFE-1 mislocalization seen here. It is evident from these results that

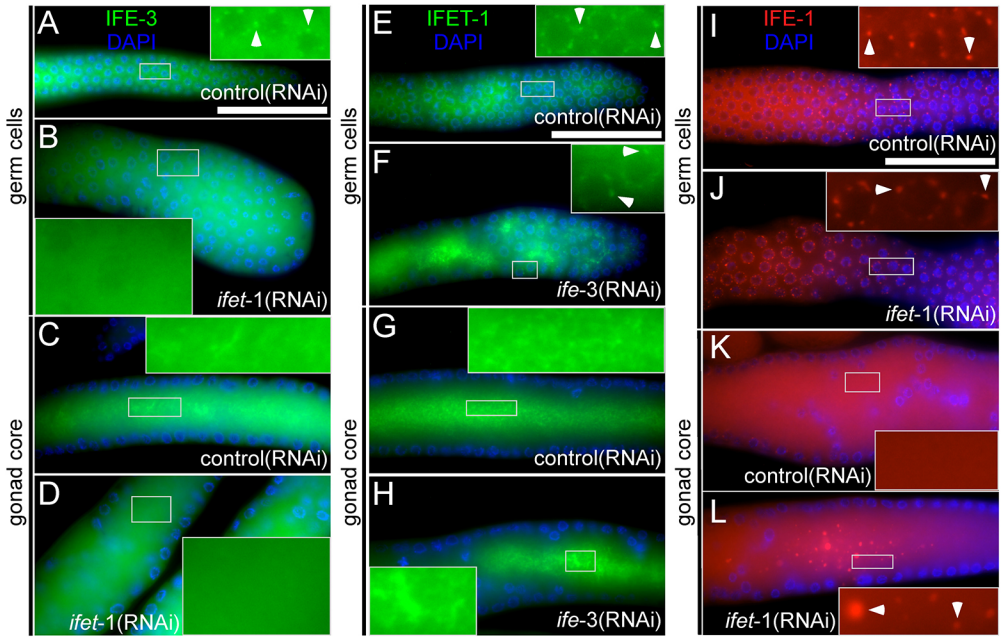

Fig. 7. IFE-3:IFET-1 localization following depletion of each subunit. (A) IFE-3 (green) expression in animals treated with control(RNAi) shows that IFE-3 forms perinuclear granules in distal germ cells (inset, arrowheads). (B) IFE-3 expression in animals treated with *ifet*-1(RNAi) shows that perinuclear IFE-3 granules are disrupted (inset). (C) IFE-3 expression in animals treated with control(RNAi) shows that IFE-3 also forms lattice-like structures in the gonad core (inset). (D) IFE-3 expression in animals treated with *ifet*-1(RNAi) shows that IFE-3 lattice-like structures in the gonad core are disrupted (inset). (E) IFET-1 (green) expression in animals treated with control(RNAi) shows that IFET-1 forms perinuclear granules in distal germ cells (inset, arrowheads). (F) IFET-1 expression in animals treated with *ife*-3(RNAi) shows that perinuclear IFET-1 granules remain intact (inset, arrowheads). (G) IFET-1 expression in animals treated with control(RNAi) shows that IFET-1 also forms lattice-like structures in the gonad core (inset). (H) IFET-1 expression in animals treated with *ife*-3(RNAi) shows that IFET-1 lattice-like structures remain intact (inset). (I) IFE-1 (red) expression in animals treated with control(RNAi) shows that IFE-1 forms perinuclear granules in distal germ cells (inset, arrowheads). (J) IFE-1 expression in animals treated with *ifet*-1(RNAi) shows that perinuclear IFE-1 granules remain intact (inset, arrowheads). (K) IFE-1 expression in animals treated with control(RNAi) shows that IFE-1 does not form structures in the gonad core (inset). (L) IFE-1 expression in animals treated with *ifet*-1(RNAi) shows that IFE-1 accumulates into aggregates in the gonad core (inset, arrowheads). We found these IFE-1 aggregates to be coincident with PGL-1 (Fig. S3H). CRISPR/Cas9 fluorescently tagged mKate2::TEV::3xmyc::IFE-1 and GFP::TEV::3xflag::IFE-3 were used to evaluate expression. Gonads were dissected, fixed, and counterstained (DAPI, blue). Scale bars: 50 µm.

Journal of Cell Science (2020) 133, jcs237990. doi:10.1242/jcs.237990

each IFE is localized by its cognate 4EBP. IFET-1 localizes IFE-3 to perinuclear granules and to structures in the gonad core, but does not contribute to normal IFE-1 localization.

Our data suggest that IFE-3 and IFET-1 work together in a functional complex to exert translational control. To address this directly, we compared the polysomal profiles of germline mRNAs following separate depletion of IFE-3 or IFET-1. Our model predicts that some GSD mRNAs will exhibit similar de-repression upon loss of either protein. Overall polysome content relative to 80S was similarly decreased by *ife*-3(RNAi) and by *ifet*-1(RNAi), indicating a modest decrease in bulk protein synthesis. Remarkably, the de-repression of *fog*-1 and *fem*-3 mRNAs was identical upon depletion of either IFE-3 or IFET-1 (Fig. 8B,C). The translation of *daz*-1 mRNA has been shown by others to be repressed by IFET-1 (Sengupta et al., 2013). We were also able to show that loss of either IFE-3 or IFET-1 caused identical *daz*-1 de-repression (Fig. 8D). Translation of IFE-1-dependent *mex*-1 mRNA and housekeeping *gpd*-3 mRNA was largely unaffected by loss of IFET-1 or IFE-3 (Fig. 8E,F). The three overlayed polysome profiles for each mRNA indicate an identical requirement for both subunits of the IFE-3: IFET-1 complex to exert translational regulation in GSD. Notably, IFE-3 is the nematode ortholog of canonical eIF4E-1, and would be expected to exert positive translational activity on some population of mRNAs, consistent with diminished polysome content following RNAi. Intriguingly, our polysome data also infer that IFET-1 (the nematode ortholog of human eIF4E-nuclear transport protein) also assists in that positive role.

DISCUSSION

Unique roles for multiple eIF4E isoforms in *C. elegans* germline

In this study, we observed unique germline phenotypes, translational functions and expression patterns of eIF4E isoforms IFE-1 and IFE-3, as well as IFET-1, the cognate 4EBP that functions with IFE-3. We previously characterized the unique functions of IFE-1 to promote spermatogenesis and oocyte maturation (Friday et al., 2015; Henderson et al., 2009). Epistasis experiments placed *ife*-1 downstream of the terminal regulator of GSD, *fog*-1, indicating that *ife*-1 is not involved in GSD per se but rather promotes the final stages of gametogenesis (Cha et al., 2012). Spermatocytes lacking IFE-1 arrest just prior to spermatid budding; oocytes are deficient in Ephrin (VAB-1) signaling (Henderson et al., 2009; Kawasaki et al., 2011). mRNAs under the control of IFE-1 in oocytes have been identified and include *pos*-1, *pal*-1, *oma*-1, *vab*-1 and *mex*-1 (Friday et al., 2015; Henderson et al., 2009). For example, IFE-1 recruits *vab*-1 mRNAs to heavy polysomes, linking it to oocyte maturation. Differential polysome array analysis between wild-type and *ife*-1(*bn127*) worms identified all IFE-1-dependent mRNAs (Friday et al., 2015). We employed similar approaches to identify IFE-2- and IFE-4-dependent mRNAs (Dinkova et al., 2005; Song et al., 2010). Initial studies on IFE-3 showed that it was essential for both embryogenesis and the sperm-to-oocyte switch in hermaphrodites (Keiper et al., 2000; Mangio et al., 2015). Here, we extend the genetic characterization of IFE-3 and find that it has roles beyond GSD (Figs 2 and 3). IFE-3 depletion by RNAi and elevated temperature in

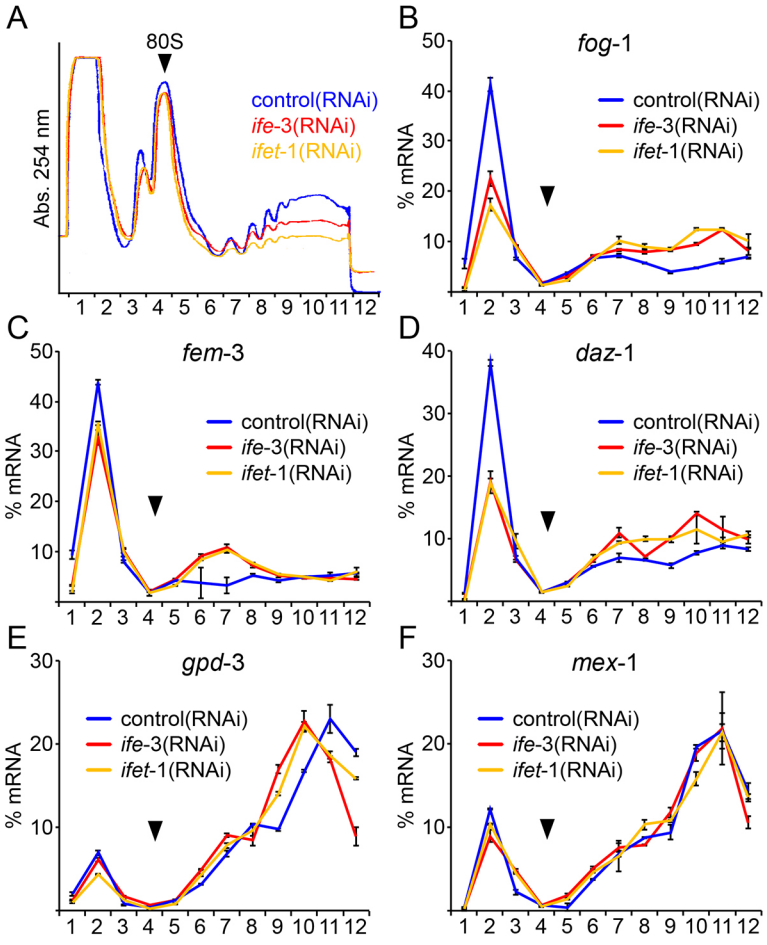

Fig. 8. Loss of IFE-3 or IFET-1 causes identical changes in GSD mRNA translation. (A) Absorbance (A_{254}) profiles for matched gradient fractionation of extracts from control(RNAi) (blue), *ife*-3(RNAi) (red) and *ifet*-1(RNAi)-treated (yellow) worms depict the polysome content. The highest resolved peak is the monosome (80S position is indicated by arrowhead) and each peak to the right represents the addition of one ribosome (polysomes). (B–F) Individual graphs depict normalized mRNA content across three matched gradients as measured by qRT-PCR for *fog*-1 (B), *fem*-3 (C), *daz*-1 (D), *gpd*-3 (E) and *mex*-1 (F) mRNAs. Normalization by total RNA content across the gradient corrects for slight differences in polysome yield, allowing direct comparison of the partitioning of each mRNA in polysomal and non-polysomal complexes. Error bars indicate the s.d. of triplicate qRT-PCR measurements.

Journal of Cell Science (2020) 133, jcs237990. doi:10.1242/jcs.237990

ife-3(*ok191*) mutants allowed bypass of the sperm-to-oocyte switch but resulted in embryonic lethality, possibly due to defects in oocyte meiosis and growth. Thus, major roles for IFE-3 are to promote the sperm-to-oocyte switch, oocyte meiosis and embryogenesis, which is a clear distinction from roles of IFE-1 in sperm cytokinesis and oocyte maturation. For instance, IFE-3 is fully dispensable for spermatogenesis, whereas IFE-1 is required (Fig. S2). Remarkably, there appear to be non-redundant functional roles for three eIF4E isoforms in the germline, where each regulates its own unique subset of mRNAs (Fig. S5) (Friday and Keiper, 2015). The mechanism by which eIF4E isoforms discriminate among mRNAs is unlikely to be due to their protein structures, which are very homologous (Keiper et al., 2000). The structure of each mRNA cap-binding protein allows for recognition of only two to three nucleotides beyond the m7G cap (Marcotrigiano et al., 1997). Although IFE-1 and IFE-3 differ somewhat in binding to m7G and 2,2,7-trimethylguanosine (m2,2,7G) caps (Miyoshi et al., 2002), the modest affinity differences are unlikely to account for the selective mRNA translational control we observe (Dinkova et al., 2005; Friday et al., 2015; Song et al., 2010). In addition, genes subject to trans-splicing give rise to heterogeneity of m7G and m2,2,7G-capped mRNAs, with the exception of downstream operon mRNAs (Blumenthal, 2005). We suggest that mRNA selectivity is based on association with unique cognate 4EBPs; namely, PGL-1 for IFE-1 and IFET-1 for IFE-3. The fact that identical translational regulation of IFE-3-responsive mRNAs was observed upon loss of IFET-1 lends strong support to this mechanistic model (Fig. 8; Fig. S5).

Roles for IFE-3 and IFET-1 in translational control of GSD mRNAs

Many of the GSD-disrupting mutations have been mapped to regulatory elements within the 3′-UTR of several genes (e.g. *fem*-3gf and *tra*-2gf alleles) (Barton et al., 1987; Goodwin et al., 1993), or were null mutations in RBP genes (*fbf* genes, *fog*-1, *gld*-1) (Barton and Kimble, 1990; Jan et al., 1999; Zhang et al., 1997). Each case pointed to mRNA repression events mediated by sequence-specific RBPs. Genetic characterization indicated a strong requirement for *ife*-3 during hermaphrodite GSD. Our epistatic analysis placed the role of *ife*-3 downstream of *fog*-2, and upstream or at the level of *fem*-3, and implicated synergistic involvement of *fbf* genes to promote oocyte fate (Fig. 3). Using polysome analysis, we identify mRNAs that IFE-3 and IFET-1 regulate in GSD and show that their role appears to include co-repression and/or activation of translation. Loss of IFE-3 led to enhanced translation initiation of repressed *fem*-3, *fog*-1, *fbf*-1/2 and *gld*-1 mRNAs. The *fem*-3 and *fog*-1 mRNAs show the most dramatic de-repression (Fig. 4), which may contribute to the involvement of IFE-3 in the sperm-to-oocyte switch. We found no evidence that IFE-3 depletion altered translational efficiency of other GSD mRNAs involved in oocyte fate (*tra*-1, *nos*-3, *mog*-1; data not shown). Importantly, translation of IFE-3-responsive GSD mRNAs was not substantially altered by loss of IFE-1 (Friday et al., 2015). However, they were de-repressed identically by depletion of IFE-3 or IFET-1 (Fig. 8). The similarity of translational outcomes and developmental defects strongly suggests a unified function for the IFE-3:IFET-1 mRNP in repression to activation switches (see Fig. 1A). Loss of IFE-3 also induced substantial new expression of *fog*-1 mRNA in larval germlines even before the sperm-to-oocyte switch occurred (Fig. 5). Additionally, *tra*-2 mRNA translational efficiency was partly dependent upon IFE-3 (Fig. 4F). However, it is also possible that enhanced *gld*-1 mRNA translation may contribute (Fig. 4E), as GLD-1 acts to repress translation of *tra*-2 (Jan et al., 1999). The translational efficiency of a known IFE-1-dependent mRNA, *mex*-1, was unperturbed by loss of IFE-3 or IFET-1 (Figs 4H and 8F), providing further evidence that each eIF4E works selectively with its own mRNA targets. Housekeeping mRNAs *gpd*-3 and *tbb*-2 appear to be impartial to any single isoform (Figs 4G and 8E) (Dinkova et al., 2005; Friday et al., 2015; Song et al., 2010). Interestingly, the mRNAs de-repressed upon IFE-3 or IFET-1 loss are also direct FBF targets (Kershner and Kimble, 2010). Combined with our genetic data, this suggests that IFE-3:IFET-1 may take part in FBF mRNP-mediated repression of some GSD mRNAs. Alternatively, IFE-3 may positively regulate an unknown factor that inhibits FBF expression or activity. Our polysome analysis showed that translation of both *fbf*-1 (Fig. 4) and *fbf*-2 mRNAs (data not shown) were de-repressed upon IFE-3 loss, supporting the latter interpretation. However, any interpretation is complicated by the finding that FBFs autoregulate their own translation (Lamont et al., 2004). If an IFE-3–FBF cooperation exists, it must exclude germline stem cell maintenance mRNAs, because we found no role for IFE-3 in regulating mitotic activity (Fig. S4) as FBFs are known to do (Crittenden et al., 2006). Patterns of IFE-3 expression place it in the right place and time to regulate GSD mRNAs.

Localization patterns of IFE-1 and IFE-3 are unique and regulated by their cognate 4EBPs

How each IFE regulates a subset of mRNAs for unique germline roles may be best explained by subcellular localization patterns. Mammalian eIF4E isoforms were shown to differentially localize to P bodies and stress granules, suggesting that they differentially regulate mRNA trafficking, translation and/or turnover (Andrei et al., 2005; Frydryskova et al., 2016). Our studies begin to put *C. elegans* eIF4E isoform-specific regulation into the context of temporal and spatial mRNP complexes (Fig. S5). We characterized two eIF4E isoforms using CRISPR/Cas9 to fluorescently tag endogenous *ife* genes. Our early transgenic studies showed that IFE-1 localized to P granules in embryos via a direct protein–protein interaction with its cognate 4EBP, PGL-1 (Amiri et al., 2001). CRISPR-tagged IFE-1 likewise localized tightly to PGL-1 granules in early germ cells, oocytes and embryos (Fig. 6). We never observed any IFE-1 foci that were not coincident with PGL-1 throughout development. Previously we described the role of IFE-1 in regulating maternal mRNAs that are also enriched in P granules (Henderson et al., 2009). Clearly, both the translational function and subcellular localization of IFE-1 are intricately tied to PGL-1. Surprisingly, CRISPR-tagged IFE-3 also resided in germ granules, which were distinct from IFE-1:PGL-1 granules (Figs 1, 6 and 7). The cognate 4EBP of IFE-3, IFET-1, is suggested to be a broad-scale translational repressor and has important functions in embryogenesis, gonad morphology and GSD (Sengupta et al., 2013). IFET-1 depletion caused dissociation of IFE-3 from both perinuclear granules and rachis structures, but IFE-3 depletion did not disrupt association of IFET-1 with those same structures (Fig. 7A–D vs E–H). This suggests a binding hierarchy in which IFET-1 directs IFE-3 localization to both structures, where they prevent translation of their bound mRNAs in localized mRNPs, and that their functions are tightly linked, like IFE-1:PGL-1. Yet their localization and translational roles appear to be distinct from the IFE-1:PGL-1 mRNPs (Figs 7 and 8). A *Drosophila* 4EBP called Cup was similarly shown to regulate the localization and inhibit function of an oocyte eIF4E isoform (Nakamura et al., 2004; Wilhelm et al., 2003), while another called Mextli enhances eIF4E-1 activity in ovarian germ cells of the fly (Hernández et al., 2013). In worms, the biochemical isolation of *in vivo* OMA-1

Journal of Cell Science (2020) 133, jcs237990. doi:10.1242/jcs.237990

mRNPs containing IFE-3 and IFET-1 also co-purify with polyadenylase (GLD-2) and CCR4–NOT deadenylase machinery (Li et al., 2009; Spike et al., 2014). OMA-1 mRNPs have roles in oocyte maturation (Spike et al., 2014). Such complexes are likely important for translational regulation by IFE-3. Curiously, the *oma-1* mRNA relies heavily on IFE-1 for efficient translation (Henderson et al., 2009), suggesting separable roles for the two eIF4Es that ensure normal translational regulation of oocyte development.

Where IFE-1 and IFE-3 are localized in separate granules, they likely sequester their preferred mRNAs from active translation in repressed mRNPs. Where both are soluble in the germ cell cytoplasm, they likely associate with eIF4G (IFG-1) to participate in mRNA translation initiation (Friday and Keiper, 2015; Keiper et al., 2000). Each IFE moves to the soluble fraction in a different cell type – IFE-1 in late spermatocytes (Fig. 6E) and IFE-3 in large oocytes (Fig. 1H,L). In each case, the relevant IFE becomes soluble at a time when its positive translation activity is expected, based on phenotype. It is well known that 4EBPs inhibit translationally productive eIF4E:eIF4G interactions (Grüner et al., 2018; Haghighat et al., 1995). We propose a model in which IFE-1 and IFE-3 have active and dormant periods that are controlled by their regional expression and cognate 4EBPs, potentially explaining how each eIF4E isoform regulates its own subset of mRNAs (Fig. S5). Dormant periods are those when each eIF4E:4EBP is associated with a unique germ granule and acts as a translational repressor. In active periods, each eIF4E leaves the germ granule and the 4EBP to exert positive initiation activity on its cargo mRNAs, recruiting them to ribosomes for translation. We do not yet have direct demonstration of each regulated mRNA that resides in an IFE-containing mRNP. The mechanisms by which 4EBPs control eIF4E repression and activation in germ cells may also involve eIF4G competition or cooperation, as well as mRNP localization, shuttling or remodeling. Our current findings are novel in characterizing two distinct eIF4E:4EBP mRNP complexes in *C. elegans* that have independent dynamics and lead to differential translational control of germline mRNAs.

MATERIALS AND METHODS

Strains and maintenance

C. elegans Bristol var. N2 was used as the wild-type strain in all experiments unless otherwise noted. DUP71 *pgl*-1(*sam33*[*pgl*-1::*gfp*::3x*flag*])IV and DUP121 *glh*-1(*sam24*[*glh*-1::*gfp*::3x*flag*])I; *pgl*-1(sam52[*pgl*-1::*mTagRFP*::3x*flag*])IV were obtained from Dr Dustin Updike (MDI Biological Laboratory, Bar Harbor, ME). Strains JK2958 nT1[*qIs51*] (IV;V)/*dpy*-11(*e224*) *unc*-42(*e270*)V, CGC20 *dpy*-18(*e364*)/eT1 III; *unc*-46(*e177*)/eT1[*umnIs9*]V, JK574 *fog*-2(*q71*)V, CB3844 *fem*-3(*e2006*)IV, JK3022 *fbf*-1(*ok91*)II, JK3101 *fbf*-2(*q738*)II, GR1373 *eri*-1(*mg366*)IV, and DG3913 *lin*-41(*tn1541*[*gfp*::*tev*::*s*::*lin*-41])I were obtained from the *Caenorhabditis* Genetics Center (University of Minnesota, Minneapolis, MN) which is funded by the NIH Office of Research Infrastructure Programs (grant number P40 OD010440). The *ife*-3(*ok191*) allele was obtained from the *C. elegans* Knockout Consortium (OMRF), outcrossed ten times to N2 worms, and balanced with *unc*-34(*e566*) to make KX10 *ife*-3(*ok191*)/*unc*-34(*e566*)V. The *ife*-3 allele was then crossed into strain JK2958 to more stably balance it with nT1[*qIs51*] to make KX98 *ife*-3(*ok191*)/nT1[*qIs51*]V, and with eT1[*umnIs9*] to make KX140 *ife*-3(*ok191*)/eT1[*umnIs9*]V. Breakpoint of *ife*-3(*ok191*) deletion was determined by subcloning and sequencing of the genomic deletion PCR product, and found to be taattttcatattttccgct/tatcta/ttatcgatttttttccagatg. KX143 *ife*-1(*eu20*[*mkate2*::*tev*::3x*myc*::*ife*-1])III, and KX152 *ife*-3(*eu21*[*gfp*::*tev*::3x*flag*::*ife*-3])V, were made using CRISPR/Cas9-driven homologous recombination to make in-frame insertions at the respective endogenous gene loci in N2 worms. KX149 *ife*-1(*eu20*[*mkate2*::*tev*::3x*myc*::*ife*-1])III, *pgl*-1(*sam33*[*pgl*-1::*gfp*::3x*flag*])IV was made by crossing KX143 and DUP75. KX155 *ife*-1(*eu20*[*mkate2*::*tev*::3x*myc*::*ife*-1])III, *ife*-3(*eu21*[*gfp*::*tev*::3x*flag*::*ife*-3])V was made by crossing KX143 and KX152. KX157 *ife*-3(*eu21*[*gfp*::*tev*::3x*flag*::*ife*-3])V, pgl-1(*sam52*[*pgl*-1::*mTagRFPT*::3x*flag*])IV was made by crossing KX152 and DUP121 and outcrossing *glh*-1(*sam24*). KX159 *ife*-3(*ok191*)/nT1[*qIs51*]V, *lin*-41(*tn1541*[*gfp*::*tev*::*s*::*lin*-41])I was made by crossing KX98 and DG3913. Strain PRB171 *qfIs012*(FL-IFET-1::*ifet*-1(*tm2944*): GFP::3XFLAG+*unc*-*119*(+)) was created by biolistic transformation of *unc*-119(*ed3*) worms (Praitis et al., 2001) with recombineered fosmid DNA generated by the *C. elegans* TransgeneOmics Project, Max Planck Institute of Molecular Cell Biology and Genetics, Dresden, Germany (Sarov et al., 2006). All strains were maintained on nematode growth medium (NGM) plates at 20°C unless otherwise indicated, with *Escherichia coli* strain OP50 as described (Brenner, 1974).

Mating and fertility experiments

Fertility of *ife*-1 and *ife*-3 mutant worms was determined at two different temperatures: permissive temperature (20°C) or restrictive temperature (25°C). To this end, *ife*-1(*bn127*), *ife*-3(*ok191*) and *fog*-2(*q71*) (control) mutant strains were grown from embryo stage at 20°C or 25°C. L4 males were transferred to new NGM plates and incubated for 24 h at 20°C or 25°C. Adult males were soaked in M9 solution with 50 µM SYTO17 red fluorescent dye (Molecular Probes) for 3 h, and each male was transferred to an OP50-seeded NGM with a single *fog*-2 female mutant worm. Twenty-four hours later, mating efficiency was determined by counting the number of *fog*-2 female worms with SYTO17(+) sperm in their spermatheca among *fog*-2 worms tested. Fertility was determined by counting the number of *fog*-2 females with SYTO17(+) sperm and embryos in the uterus.

Characterizing *ife*-3(*ok191*) temperature-sensitive fertility rescue

To unambiguously determine the frequency of the temperature-sensitive rescue of *ife*-3(*ok191*) fertility and separate poorly balanced *ife*-3 genetic recombinants from true *ife*-3(−/−) animals at 25°C, we generated synchronized populations of KX98 *ife*-3(*ok191*)/nT1[*qIs51*]V worms by using a solution of NaClO (1.3%) and NaOH (0.5 M) on gravid hermaphrodites, hatching F_1 embryos overnight in M9 at 20°C and seeding L1 larva onto NGM plates with OP50 to be grown at 20°C or 25°C. Twenty-four hours after L4 molting, animals were dissected with a 30-gauge needle under a stereomicroscope to determine if they were fertile (embryos) or sterile (no embryos), then individual worms were collected for genomic PCR using the following triple primer set: forward 1, 5′-TATGTGCATGTTGTGGAGGCTG-3′; reverse, 5′-TGTAGTCTCCGTACTCGTCG-3′; forward 2, 5′-CAGAATCGCTGGGCTCTC-3′, yielding a single 417 bp product in *ife*-3(+/+) worms, a single 756 bp product in *ife*-3(−/−) worms and both products in *ife*-3(+/−) worms. Results were pooled from three individual experiments.

RNAi

Gene-specific RNAi was performed by feeding *C. elegans* with double-stranded RNA (dsRNA) expressing *E. coli* (HT115) as described, with minor modifications (Timmons et al., 2001; Timmons and Fire, 1998). Briefly, HT115 was transformed with either L4440 vector or gene-specific constructs and grown overnight at 37°C in 2xYT medium containing 50 µg/µl carbenicillin. Cultures were concentrated 5-fold by centrifugation, seeded onto nematode growth medium (NGM) plates containing 1 mM IPTG and 50 µg/µl carbenicillin, then induced overnight at room temperature before plating worms. dsRNA was extracted from bacterial plates after induction and run on denaturing 2% agarose gels with ethidium bromide to determine dsRNA expression when appropriate. For feeding, L4 hermaphrodites were seeded onto RNAi plates and F_1 offspring were evaluated for phenotype (Fig. 3) or processed for biochemical analysis (polysomes; Fig. 4). RNAi feeding experiments were conducted at 25°C, with the exception that CB3844 *fem*-3(*e2006*) and GR1373 *eri*-1(*mg366*) L4 mothers were grown at 20°C for the first 24 h of feeding, then shifted to 25°C, due to decreased fertility at higher temperatures. We generated the *ife*-3(RNAi) feeding construct (pT72-*ife*-3) by inserting a 475 bp restriction-digested *ife*-3 complementary DNA (cDNA) fragment containing only the coding region (Jankowska-Anyszka et al., 1998) into the L4440 vector backbone using standard cloning procedures. We also generated *ifet*-1(RNAi) feeding construct (pT72-*ifet*-1)

Journal of Cell Science (2020) 133, jcs237990. doi:10.1242/jcs.237990

by inserting a 600 bp PCR-amplified *ifet*-1 fragment into the L4440 vector backbone, again using standard cloning procedures (Maniatis et al., 1989). The *fog*-1(RNAi) construct has been previously described (Datla et al., 2014). The identity of RNAi clones was verified via Sanger sequencing (Iowa State Sequencing Facility).

CRISPR/Cas9 genome editing

CRISPR/Cas9 mediated genome editing was accomplished by using pDD162 (plasmid #47549, Addgene) to express single-guide RNA (sgRNA) driven by *C. elegans* U6 promoter and Cas9 DNA endonuclease protein under control of the *eef*-1A.1/*eft*-3 promoter, in conjunction with plasmid-based homology directed repair (HDR) template containing a self-excising cassette (SEC), as described with minor modifications (Dickinson et al., 2015, 2013). We generated multiple pDD162 sgRNA/Cas9-expressing plasmids for *ife*-1 and *ife*-3, using a Q5® site-directed mutagenesis kit from New England Biolabs (NEB) as per the manufacturer's instructions. We also generated HDR templates for *ife*-1 and *ife*-3 by inserting PCR-amplified homology arms (~550–950 bp) corresponding to upstream and downstream regions of each gene relative to the start codon (ATG) into pDD287 and pDD282 backbones (plasmid #70685 and #66823, Addgene), respectively, using a Gibson Assembly® kit (NEB) as per the manufacturer's instructions. When possible, conserved mutations were made in protospacer adjacent motif (PAM) sites within the homology arms to prevent HDR template cutting by Cas9; when mutation of the PAM site was not possible, conserved mutations were incorporated throughout the sgRNA target site. sgRNA/Cas9-expressing plasmids and HDR template plasmids were isolated using a PureLink® Miniprep Kit (Invitrogen) as per the manufacturer's instructions and confirmed via Sanger sequencing (Iowa State Sequencing Facility). We injected mated N2 hermaphrodites as young adults in order to increase brood sizes. Injection cocktails were as follows: *ife*-1 injection mix: pDD162-*ife*-1-256 (sgRNA/Cas9 50 ng/µl), pDD287-*ife*-1 (HDR SEC 10 ng/µl), pPD118.2 (GFP co-injection marker 5 ng/µl); *ife*-3 injection mix: pDD162-*ife*-3-181, pDD162-*ife*-3-7741, pDD162-*ife*-3-8300 (each sgRNA/Cas9 25 ng/µl), pDD287-*ife*-3 (HDR SEC 10 ng/µl), pCJ104 (RFP co-injection marker 5 ng/µl). Progeny of injected worms were selected with Hygromycin (final concentration 250 µg/ml) at 20°C and screened for survival, Rol phenotype and lack of co-injection marker, then heat shocked at 34°C for 3–4 h to remove SEC. Non-rollers from heat shock plates were screened by genomic PCR to confirm insertion at the desired locus. Animals containing the desired insertion were backcrossed at least three times to N2 males. N-terminal protein fusions did not appear to grossly affect IFE-1 and IFE-3 function as worms homozygous for both insertions were superficially wild type and had wild-type fertility.

Microscopy and immunostaining

Dissection of hermaphrodite or male germlines and immunostaining were performed as described with minor modifications (Cha et al., 2012). For MSP immunostaining, worms of the indicated genotype and treatment were dissected under a stereomicroscope using a 30-gauge needle, germlines were fixed in 3% paraformaldehyde in 1× phosphate buffered saline (PBS; pH 7.2) for 20 min at room temperature, washed in PBS+0.01% Tween 20 (PTW), then post-fixed in ice cold 100% MeOH and stored at −20°C. Following fixation, dissected germlines were rehydrated in 50% cold MeOH, washed in PTW, blocked for 1 h in PTW+0.5% bovine serum albumin (PTWB) at room temperature, incubated with mouse anti-MSP (1:100) primary antibody (Yoon et al., 2016) in PTWB overnight at 4°C, washed in PTWB extensively, then incubated in Alexa Fluor 488- or Alexa Fluor 568-conjugated goat anti-mouse-IgG (1:400) secondary antibody (Invitrogen) in PTWB for 1 h at room temperature. They then underwent a final incubation in DAPI for 15 min at room temperature before being washed extensively in PTWB and mounted on 2% agarose imaging pads in 90% glycerol/DABCO (ACROS Organics) anti-fade medium. For imaging CRISPR/Cas9 endogenously tagged fluorescent protein fusions, we replaced the 100% MeOH post-fix and rehydration step above with a 70% EtOH post-fix and rehydration step, and did not block in PTWB or use immunostaining; other steps for fixing and imaging these germlines was identical to those described above. We also imaged CRISPR/Cas9 fusions in live worms treated with NaN_3 (2 mM) and levamisole (5 mM) for immobilization. Germline imaging was performed on a Zeiss Axiovert 200M Differential Interference Contrast (DIC) microscope equipped with an Axiocam MRm CCD camera and corresponding DAPI/Hoechst, and FITC/GFP, and TexasRed/RFP optics with 40× air or 100× oil objectives. Image processing was performed using Axiovision 4.3 software (Carl Zeiss). Any image adjustments to contrast or brightness were conducted linearly.

Analysis of polysomes by sucrose gradient fractionation

Lysis and gradient buffers, gradient setup, centrifugation and fractionation were conducted as described with the following modifications (Dinkova et al., 2005; Henderson et al., 2009). L4-stage N2 hermaphrodites were seeded onto NGM plates with HT115 expressing either L4440(RNAi), *ife*-3(RNAi) or *ifet*-1(RNAi) and allowed to grow at 25°C for ~96 h until plates were saturated with mix-staged F_1 and F_2 progeny. We estimate that young adult worms composed >75% of the biomass on each plate. Worms were then washed off plates using M9, allowed to purge gut contents for 30 min in M9, and floated in 35% sucrose at 4°C to remove debris and bacteria, then flash frozen in liquid nitrogen in the presence of 14 mM E64 protease inhibitor (Sigma-Aldrich) and 4 mM Vanadyl-RNC RNase inhibitor (Sigma-Aldrich). Worms were crushed in a mortar and pestle under liquid N_2 with an equal volume of buffer A [50 mM Tris-HCl pH 8.0, 300 mM NaCl, 10 mM $MgCl_2$, 1 mM EGTA, 2 mM dithiothreitol (DTT), 800 U of RNAsin/ml (Promega), 4 mM Vanadyl-RNC, 5 mM PMSF, 0.4 mg/mL Cycloheximide (Calbiochem)], and centrifuged at 14,000 ***g*** at 4°C for 15 min. A 0.5-ml aliquot of the supernatant was applied to an 11-ml 10–45% linear sucrose density gradient made in buffer B (25 mM Tris-HCl pH 8.0, 140 mM NaCl, 10 mM $MgCl_2$, 1 mM DTT) and centrifuged in a Beckman SW41Ti rotor at 38,000 rpm at 4°C for 2 h. Gradients were fractionated into 1 ml fractions with continuous monitoring of absorbance at 254 nm with an ISCO UA-6 UV VIS detector. Sucrose fractions were stored at −80°C prior to use.

Quantitative reverse transcription PCR (qRT-PCR) on sucrose gradient fractions

RNA from sucrose gradient fractions was isolated in four volumes of Trizol® Reagent (Thermo Fisher Scientific) as per the manufacturer's instructions with the following additions: after isopropanol precipitation, fractions were extracted once with phenol-chloroform-iso-amyl alcohol (25:24:1), then extracted once with chloroform-isoamyl alcohol (24:1), followed by EtOH precipitation at 4°C overnight with 20 µg glycogen (Thermo Fisher Scientific). RNA was isolated from 500 µl of each 1-ml gradient fraction. RNA concentrations were measured on a NanoDrop® ND-1000 spectrophotometer and assessed for RNA purity based on A260/280 ratios. cDNA was synthesized from each fraction using an iScript Advanced cDNA Synthesis Kit (Bio-Rad) using 0.4 µg of input RNA as per the manufacturer's instructions. qRT-PCR was performed in triplicate on a CFX Real-Time System (Bio-Rad) using Sso Fast Evagreen Super mix (Bio-Rad), according to the manufacturer's instructions. qRT-PCR quantification of each mRNA was normalized to total RNA content. Standard curves were generated for each primer set and used for absolute quantification. Similar traces were obtained for *fem*-3, *fog*-1 and *gpd*-3 mRNAs (Fig. 3) on two to three independent gradients. Primer sequences used were as follows: *tbb*-2 (forward, 5′-TCATCTCCAAAATCCGCGAA-3′; reverse, 5′-GAGGGATACAAGATGGTTC-3′); *mex*-1 (forward, 5′-AATGGATAAGCTAATGTTGGA-3′; reverse, 5′-GATATTGCGATGAGGAAGAG-3′); *fem*-3 (forward, 5′-AAGCTGACAGAGAAACGAGA-3′; reverse, 5′-AAAGGAATTCCAGATATTAAAGG-3′); *fbf*-1 (forward, 5′-GACCAATCAAAAATGCGCTAT-3′; reverse, 5′-GATTTCCAACCTCTGTAGATGTG-3′); *fog*-1 (forward, 5′-TCAGTGCCAGGATTTAGAGA-3′; reverse, 5′-AATATCGATGATACGGTTGTG-3′); *gld*-1 (forward, 5′-TTCAGGTCCAGTTTTGATGT-3′; reverse, 5′-GACGTTAGATCCGAGAAGGT-3′); *daz*-1 (forward, 5′-ACAAAAAGCCCAATCAAAG-3′; reverse, 5′-GCTGAAAGTGGAGAAAGATG-3′); *gpd*-3 (forward, 5′-GATCTCAGCTGGGTCTCTT-3′; reverse, 5′-TCCAGTACGATTCCACTCAC-3′); and *tra*-2 (forward, 5′-TTCAATTGCAACAAAACAAA-3′; reverse, 5′-TCTGCACCAAATTGTAGACC-3′).

Micro-scale qRT-PCR

We conducted micro-scale qRT-PCR on whole-worm lysates as described with minor modifications (Contreras et al., 2008). We generated

synchronized populations of N2 and KX98 *ife*-3(*ok191*)/nT1[*qIs51*]V worms using a solution of NaClO (1.3%) and NaOH (0.5 M) on gravid hermaphrodites, hatching F_1 eggs overnight in M9 at 20°C, and seeding L1 larvae onto NGM plates with OP50 to be grown at 20°C. Three independent biological replicates each containing ∼25 early or late L4 hermaphrodites (N2 or *ife*-3−/−) were collected into 25 µl of single-worm lysis buffer (15 mM Tris-HCl pH 8.0, 50 mM KCl, 1 mM $MgCl_2$, 0.45% NP-40, 0.45% Tween 20) containing 0.2 mg/ml Proteinase K (60 min at 60°C; 10 min at 95°C). Upon completion of lysis, RNA was isolated using the PureLink® RNA Mini Kit (Invitrogen) with on-column DNAse I digestion, followed by EtOH precipitation at −20°C overnight with 20 µg glycogen (Thermo Fisher Scientific). RNA was resuspended in 10 µl of nuclease free H_2O for cDNA synthesis and qRT-PCR as described above. Reactions were conducted in triplicate from three independent biological replicates, quantified and normalized to *tbb*-2 (endogenous control) using the $2^{-\Delta\Delta Ct}$ method. Student's *t*-test was used to determine statistical significance between *ife*-3(−/−) and wild-type animals, with a *P*-value cutoff of 0.05.

5-Ethynyl-2′-deoxyuridine (EdU) labeling and measuring S-phase indices

Metabolic labeling of DNA synthesis was performed as described with minor modifications (Yoon et al., 2018). Animals were incubated in M9+0.1% Tween 20 with 1 mM EdU for 30 min at 20°C. Gonads were dissected and fixed in 3% paraformaldehyde solution in 0.1 m K_2HPO_4 (pH 7.2) for 10–20 min, followed by −20°C methanol fixation for 10 min. Dissected gonads were blocked in PTWB solution for 30 min at 20°C. EdU labeling was detected using a Click-iT EdU Alexa Fluor 488 Imaging Kit (Invitrogen) according to the manufacturer's instructions. After washing 3× with PTWB solution for at least 30 min at 10 min intervals, the dissected gonads were stained with a final incubation in DAPI for 15 min at room temperature before being washed extensively in PTWB and mounted on 2% agarose imaging pads in 90% glycerol/DABCO (ACROS Organics) anti-fade medium.

Western blot analysis

Frozen worm pellets used for polysome analysis (Fig. 3) were ground in liquid nitrogen in CL+ buffer [40 mM MOPS pH 7.5, 200 mM KCl, 2 nM EDTA, 4 mM EGTA, 2 mM DTT, 14 mM E64 and HALT protease cocktail (Thermo Fisher Scientific)], and centrifuged at 14,000 ***g*** for 10 min. The supernatant was batch bound to m7G sepharose (Sigma-Aldrich) beads for 1 h at 4°C, washed 3× with CL+, boiled in 2× SDS load buffer for 3 min, and 30 µg protein for each sample was resolved by 12% SDS-PAGE. Proteins were transferred to polyvinylidene fluoride (PVDF) membranes overnight and blocked with TST (10 mM Tris-HCl pH 7.4, 150 mM NaCl, 0.05% Tween 20) containing 5% dry non-fat milk for 1 h at room temperature, then incubated with a 1:1000 dilution of an IFE-3-specific primary antibody CA82 (Jankowska-Anyszka et al., 1998) in TST containing 5% dry non-fat milk for 1 h at room temperature. Blots were washed 5× in TST containing 5% dry non-fat milk and incubated with a 1:10,000 dilution of goat anti-rabbit IgG secondary antibody conjugated to horseradish peroxidase (HRP) in TST containing 5% dry non-fat milk for 1 h at room temperature, then washed extensively. Detection was performed with an ECL+ kit (Thermo Fisher Scientific) according to the manufacturer's instructions. Image acquisition was performed using an Amersham Typhoon Fluorescence/Phosphorimaging scanner (GE Healthcare) at the ECU PhIFI Core Facility.

Acknowledgements

We thank Dan Dickinson (University of Texas at Austin) for advice on CRISPR/Cas9 gene editing, Dustin Updike (MDI Biological Laboratory, Bar Harbor, ME) for fluorescent PGL-1 CRISPR strains, Sammy Chouffani for subcloning the *ifet*-1(RNAi) plasmid and Caitlin Palmer for preliminary experiments. We thank the *C. elegans* Gene Knockout Consortium at OMRF for the original mutant isolate of *ife*-3(*ok191*) and Dr Mihail Sarov of the *C. elegans* TransgeneOme Project for the IFET-1::GFP::3xFLAG fosmid. The *fbf*-1 and *fbf*-2 strains were provided by Judith Kimble (University of Wisconsin). The *fem*-3, *fog*-2, *eri*-1 and *lin*-41(*tn1541*[*gfp*::*tev*::*s*::*lin*-41]) strains were from the *Caenorhabditis* Genetics Center, funded by the NIH Office of Research Infrastructure Programs [P40 OD010440].

Competing interests

The authors declare no competing or financial interests.

Author contributions

Conceptualization: H.P.H., M.A.H., M.-H.L., B.D.K.; Methodology: H.P.H., J.S.S., J.L.H., D.S.B., M.S.S., P.R.B., M.-H.L., B.D.K.; Validation: B.D.K.; Formal analysis: H.P.H., H.S., M.A.H., J.L.H., M.-H.L., B.D.K.; Investigation: H.P.H., J.S.S., H.S., M.A.H., J.L.H., D.S.B., P.R.B., M.-H.L., B.D.K.; Resources: B.D.K.; Data curation: H.P.H., B.D.K.; Writing - original draft: H.P.H., B.D.K.; Writing - review & editing: H.P.H., M.A.H., J.L.H., P.R.B., M.-H.L., B.D.K.; Visualization: H.P.H., B.D.K.; Supervision: B.D.K.; Project administration: M.-H.L., B.D.K.; Funding acquisition: M.A.H., M.-H.L., B.D.K.

Funding

This work was supported by the National Science Foundation [MCB-1714264 and MCB-0842475 to B.D.K.] and the National Institutes of Health [AG060373 to M.-H.L.]. Deposited in PMC for release after 12 months.

Supplementary information

Supplementary information available online at
http://jcs.biologists.org/lookup/doi/10.1242/jcs.237990.supplemental

Peer review history

The peer review history is available online at
https://jcs.biologists.org/lookup/doi/10.1242/jcs.237990.reviewer-comments.pdf

References

Amiri, A., Keiper, B. D., Kawasaki, I., Fan, Y., Kohara, Y., Rhoads, R. E. and Strome, S. (2001). An isoform of eIF4E is a component of germ granules and is required for spermatogenesis in *C. elegans*. *Development* **128**, 3899-3912.

Andrei, M. A., Ingelfinger, D., Heintzmann, R., Achsel, T., Rivera-Pomar, R. and Luhrmann, R. (2005). A role for eIF4E and eIF4E-transporter in targeting mRNPs to mammalian processing bodies. *RNA* **11**, 717-727. doi:10.1261/rna.2340405

Barton, M. K. and Kimble, J. (1990). *fog-1*, a regulatory gene required for specification of spermatogenesis in the germ line of *Caenorhabditis elegans*. *Genetics* **125**, 29-39.

Barton, M. K., Schedl, T. B. and Kimble, J. (1987). Gain-of-function mutations of fem-3, a sex-determination gene in Caenorhabditis elegans. *Genetics* **115**, 107-119.

Blumenthal, T. (2005). Trans-splicing and operons. *WormBook*, 1-9.

Brenner, S. (1974). The genetics of Caenorhabditis elegans. *Genetics* **77**, 71-94.

Cha, D. S., Datla, U. S., Hollis, S. E., Kimble, J. and Lee, M.-H. (2012). The Ras-ERK MAPK regulatory network controls dedifferentiation in Caenorhabditis elegans germline. *Biochim. Biophys. Acta* **1823**, 1847-1855. doi:10.1016/j.bbamcr.2012.07.006

Ciosk, R., DePalma, M. and Priess, J. R. (2006). Translational regulators maintain totipotency in the Caenorhabditis elegans germline. *Science* **311**, 851-853. doi:10.1126/science.1122491

Clifford, R., Lee, M. H., Nayak, S., Ohmachi, M., Giorgini, F. and Schedl, T. (2000). FOG-2, a novel F-box containing protein, associates with the GLD-1 RNA binding protein and directs male sex determination in the C. elegans hermaphrodite germline. *Development* **127**, 5265-5276. doi:10.3410/f.718490079.793497242

Contreras, V., Richardson, M. A., Hao, E. and Keiper, B. D. (2008). Depletion of the cap-associated isoform of translation factor eIF4G induces germline apoptosis in C. elegans. *Cell Death Differ.* **15**, 1232-1242. doi:10.1038/cdd.2008.46

Crittenden, S. L., Troemel, E. R., Evans, T. C. and Kimble, J. (1994). GLP-1 is localized to the mitotic region of the *C. elegans* germ line. *Development* **120**, 2901-2911.

Crittenden, S. L., Leonhard, K. A., Byrd, D. T. and Kimble, J. (2006). Cellular analyses of the mitotic region in the Caenorhabditis elegans adult germ line. *Mol. Biol. Cell* **17**, 3051-3061. doi:10.1091/mbc.e06-03-0170

Datla, U. S., Scovill, N. C., Brokamp, A. J., Kim, E., Asch, A. S. and Lee, M.-H. (2014). Role of PUF-8/PUF protein in stem cell control, sperm-oocyte decision and cell fate reprogramming. *J. Cell. Physiol.* **229**, 1306-1311. doi:10.1002/jcp.24618

Dickinson, D. J., Ward, J. D., Reiner, D. J. and Goldstein, B. (2013). Engineering the Caenorhabditis elegans genome using Cas9-triggered homologous recombination. *Nat. Methods* **10**, 1028-1034. doi:10.1038/nmeth.2641

Dickinson, D. J., Pani, A. M., Heppert, J. K., Higgins, C. D. and Goldstein, B. (2015). Streamlined genome engineering with a self-excising drug selection cassette. *Genetics* **200**, 1035-1049. doi:10.1534/genetics.115.178335

Dinkova, T. D., Keiper, B. D., Korneeva, N. L., Aamodt, E. J. and Rhoads, R. E. (2005). Translation of a small subset of Caenorhabditis elegans mRNAs is dependent on a specific eukaryotic translation initiation factor 4E isoform. *Mol. Cell. Biol.* **25**, 100-113. doi:10.1128/MCB.25.1.100-113.2005

Dostie, J., Ferraiuolo, M., Pause, A., Adam, S. A. and Sonenberg, N. (2000). A novel shuttling protein, 4E-T, mediates the nuclear import of the mRNA 5′ cap-binding protein, eIF4E. *EMBO J.* **19**, 3142-3156. doi:10.1093/emboj/19.12.3142

Friday, A. J. and Keiper, B. D. (2015). Positive mRNA translational control in germ cells by initiation factor selectivity. *Biomed. Res. Int.* **2015**, e327963. doi:10.1155/2015/327963

Friday, A. J., Henderson, M. A., Morrison, J. K., Hoffman, J. L. and Keiper, B. D. (2015). Spatial and temporal translational control of germ cell mRNAs mediated by the eIF4E isoform IFE-1. *J. Cell Sci.* **128**, 4487-4498. doi:10.1242/jcs.172684

Frydryskova, K., Masek, T., Borcin, K., Mrvova, S., Venturi, V. and Pospisek, M. (2016). Distinct recruitment of human eIF4E isoforms to processing bodies and stress granules. *BMC Mol. Biol.* **17**, 21. doi:10.1186/s12867-016-0072-x

Ghosh, S. and Lasko, P. (2015). Loss-of-function analysis reveals distinct requirements of the translation initiation factors eIF4E, eIF4E-3, eIF4G and eIF4G2 in Drosophila spermatogenesis. *PLoS ONE* **10**, e0122519. doi:10.1371/journal.pone.0122519

Gingras, A.-C., Raught, B., Gygi, S. P., Niedzwiecka, A., Miron, M., Burley, S. K., Polakiewicz, R. D., Wyslouch-Cieszynska, A., Aebersold, R. and Sonenberg, N. (2001). Hierarchical phosphorylation of the translation inhibitor 4E-BP1. *Genes Dev.* **15**, 2852-2864. doi:10.1101/gad.13.11.1422

Goodwin, E. B., Okkema, P. G., Evans, T. C. and Kimble, J. (1993). Translational regulation of *tra*-2 by its 3′ untranslated region controls sexual identity in *C. elegans*. *Cell* **75**, 329-339. doi:10.1016/0092-8674(93)80074-O

Grüner, S., Weber, R., Peter, D., Chung, M.-Y., Igreja, C., Valkov, E. and Izaurralde, E. (2018). Structural motifs in eIF4G and 4E-BPs modulate their binding to eIF4E to regulate translation initiation in yeast. *Nucleic Acids Res.* **46**, 6893-6908. doi:10.1093/nar/gky542

Haghighat, A., Mader, S., Pause, A. and Sonenberg, N. (1995). Repression of cap-dependent translation by 4E-binding protein 1: competition with p220 for binding to eukaryotic initiation factor-4E. *EMBO J.* **14**, 5701-5709. doi:10.1002/j.1460-2075.1995.tb00257.x

Henderson, M. A., Cronland, E., Dunkelbarger, S., Contreras, V., Strome, S. and Keiper, B. D. (2009). A germline-specific isoform of eIF4E (IFE-1) is required for efficient translation of stored mRNAs and maturation of both oocytes and sperm. *J. Cell Sci.* **122**, 1529-1539. doi:10.1242/jcs.046771

Hernández, G., Altmann, M., Sierra, J. M., Urlaub, H., del Corral, R. D., Schwartz, P. and Rivera-Pomar, R. (2005). Functional analysis of seven genes encoding eight translation initiation factor 4E (eIF4E) isoforms in Drosophila. *Mech. Dev.* **122**, 529-543. doi:10.1016/j.mod.2004.11.011

Hernandez, G., Miron, M., Han, H., Liu, N., Magescas, J., Tettweiler, G., Frank, F., Siddiqui, N., Sonenberg, N. and Lasko, P. (2013). Mextli is a novel eukaryotic translation initiation factor 4E-binding protein that promotes translation in Drosophila melanogaster. *Mol. Cell. Biol.* **33**, 2854-2864. doi:10.1128/MCB.01354-12

Hodgkin, J. (1986). Sex determination in the nematode C. elegans: analysis of tra-3 suppressors and characterization of fem genes. *Genetics* **114**, 15-52.

Jan, E., Motzny, C. K., Graves, L. E. and Goodwin, E. B. (1999). The STAR protein, GLD-1, is a translational regulator of sexual identity in *Caenorhabditis elegans*. *EMBO J.* **18**, 258-269. doi:10.1093/emboj/18.1.258

Jankowska-Anyszka, M., Lamphear, B. J., Aamodt, E. J., Harrington, T., Darzynkiewicz, E., Stolarski, R. and Rhoads, R. E. (1998). Multiple isoforms of eukaryotic protein synthesis initiation factor 4E in *Caenorhabditis elegans* can distinguish between, mono- and trimethylated mRNA cap structures. *J. Biol. Chem.* **273**, 10538-10542. doi:10.1074/jbc.273.17.10538

Joshi, B., Lee, K., Maeder, D. L. and Jagus, R. (2005). Phylogenetic analysis of eIF4E-family members. *BMC Evol. Biol.* **5**, 1-20. doi:10.1186/1471-2148-5-48

Kawasaki, I., Shim, Y.-H., Kirchner, J., Kaminker, J., Wood, W. B. and Strome, S. (1998). PGL-1, a predicted RNA-binding component of germ granules, is essential for fertility in *C. elegans*. *Cell* **94**, 635-645. doi:10.1016/S0092-8674(00)81605-0

Kawasaki, I., Jeong, M.-H. and Shim, Y.-H. (2011). Regulation of sperm-specific proteins by IFE-1, a germline-specific homolog of eIF4E, in C. elegans. *Mol. Cells* **31**, 191-197. doi:10.1007/s10059-011-0021-y

Keiper, B. (2019). Cap-independent mRNA translation in germ cells. *Int. J. Mol. Sci.* **20**, 173. doi:10.3390/ijms20010173

Keiper, B. D., Gan, W. and Rhoads, R. E. (1999). Protein synthesis initiation factor 4G. *Int. J. Biochem. Cell Biol.* **31**, 37-41. doi:10.1016/S1357-2725(98)00130-7

Keiper, B. D., Lamphear, B. J., Deshpande, A. M., Jankowska-Anyszka, M., Aamodt, E. J., Blumenthal, T. and Rhoads, R. E. (2000). Functional characterization of five eIF4E isoforms in Caenorhabditis elegans. *J. Biol. Chem.* **275**, 10590-10596. doi:10.1074/jbc.275.14.10590

Kershner, A. M. and Kimble, J. (2010). Genome-wide analysis of mRNA targets for Caenorhabditis elegans FBF, a conserved stem cell regulator. *Proc. Natl. Acad. Sci. USA* **107**, 3936-3941. doi:10.1073/pnas.1000495107

King, H. A. and Gerber, A. P. (2014). Translatome profiling: methods for genome-scale analysis of mRNA translation. *Brief Funct. Genomics* **15**, 22-31. doi:10.1093/bfgp/elu045

Lai, F., Zhou, Y., Luo, X., Fox, J. and King, M. L. (2011). Nanos1 functions as a translational repressor in the Xenopus germline. *Mech. Dev.* **128**, 153-163. doi:10.1016/j.mod.2010.12.001

Lamont, L. B., Crittenden, S. L., Bernstein, D., Wickens, M. and Kimble, J. (2004). FBF-1 and FBF-2 regulate the size of the mitotic region in the C. elegans germline. *Dev. Cell* **7**, 697-707. doi:10.1016/j.devcel.2004.09.013

Li, W., DeBella, L. R., Guven-Ozkan, T., Lin, R. and Rose, L. S. (2009). An eIF4E-binding protein regulates katanin protein levels in C. elegans embryos. *J. Cell Biol.* **187**, 33-42. doi:10.1083/jcb.200903003

Luitjens, C., Gallegos, M., Kraemer, B., Kimble, J. and Wickens, M. (2000). CPEB proteins control two key steps in spermatogenesis in C. elegans. *Genes Dev.* **14**, 2596-2609. doi:10.1101/gad.831700

Mangio, R. S., Votra, S. and Pruyne, D. (2015). The canonical eIF4E isoform of C. elegans regulates growth, embryogenesis, and germline sex-determination. *Biol. Open.* **4**, 843-851. doi:10.1242/bio.011585

Maniatis, T., Fritsch, E. F. and Sambrook, J. (1989). *Molecular Cloning: A Laboratory Manual*. Cold Spring Harbor, NY: Cold Spring Harbor Laboratory.

Marcotrigiano, J., Gingras, A.-C., Sonenberg, N. and Burley, S. K. (1997). Cocrystal structure of the messenger RNA 5′ cap-binding protein (eIF4E) bound to 7-methyl-GDP. *Cell* **89**, 951-961. doi:10.1016/S0092-8674(00)80280-9

Mehra, A., Gaudet, J., Heck, L., Kuwabara, P. E. and Spence, A. M. (1999). Negative regulation of male development in Caenorhabditis elegans by a protein-protein interaction between TRA-2A and FEM-3. *Genes Dev.* **13**, 1453-1463. doi:10.1101/gad.13.11.1453

Miyoshi, H., Dwyer, D. S., Keiper, B. D., Jankowska-Anyszka, M., Darzynkiewicz, E. and Rhoads, R. E. (2002). Discrimination between mono- and trimethylated cap structures by two isoforms of *Caenorhabditis elegans* eIF4E. *EMBO J.* **21**, 4680-4690. doi:10.1093/emboj/cdf473

Nakamura, A., Sato, K. and Hanyu-Nakamura, K. (2004). Drosophila cup is an eIF4E binding protein that associates with Bruno and regulates oskar mRNA translation in oogenesis. *Dev. Cell* **6**, 69-78. doi:10.1016/S1534-5807(03)00400-3

Patrick, R. M. and Browning, K. S. (2012). The eIF4F and eIFiso4F complexes of plants: an evolutionary perspective. *Comp. Funct. Genomics* **2012**, 287814. doi:10.1155/2012/287814

Pillai, R. S., Bhattacharyya, S. N. and Filipowicz, W. (2007). Repression of protein synthesis by miRNAs: how many mechanisms? *Trends Cell Biol.* **17**, 118-126. doi:10.1016/j.tcb.2006.12.007

Praitis, V., Casey, E., Collar, D. and Austin, J. (2001). Creation of low-copy integrated transgenic lines in Caenorhabditis elegans. *Genetics* **157**, 1217-1226.

Rhoads, R. E. (1993). Regulation of eukaryotic protein synthesis by initiation factors. *J. Biol. Chem.* **268**, 3017-3020.

Rybarska, A., Harterink, M., Jedamzik, B., Kupinski, A. P., Schmid, M. and Eckmann, C. R. (2009). GLS-1, a novel P granule component, modulates a network of conserved RNA regulators to influence germ cell fate decisions. *PLoS Genet.* **5**, e1000494. doi:10.1371/journal.pgen.1000494

Sarov, M., Schneider, S., Pozniakovski, A., Roguev, A., Ernst, S., Zhang, Y., Hyman, A. A. and Stewart, A. F. (2006). A recombineering pipeline for functional genomics applied to Caenorhabditis elegans. *Nat. Methods* **3**, 839-844. doi:10.1038/nmeth933

Schedl, T. and Kimble, J. (1988). fog-2, a germ-line-specific sex determination gene required for hermaphrodite spermatogenesis in Caenorhabditis elegans. *Genetics* **119**, 43-61.

Sengupta, M. S., Low, W. Y., Patterson, J. R., Kim, H.-M., Traven, A., Beilharz, T. H., Colaiacovo, M. P., Schisa, J. A. and Boag, P. R. (2013). ifet-1 is a broad-scale translational repressor required for normal P granule formation in C. elegans. *J. Cell Sci.* **126**, 850-859. doi:10.1242/jcs.119834

Sheth, U., Pitt, J., Dennis, S. and Priess, J. R. (2010). Perinuclear P granules are the principal sites of mRNA export in adult C. elegans germ cells. *Development* **137**, 1305-1314. doi:10.1242/dev.044255

Shimada, M., Yokosawa, H. and Kawahara, H. (2006). OMA-1 is a P granules-associated protein that is required for germline specification in Caenorhabditis elegans embryos. *Genes Cells* **11**, 383-396. doi:10.1111/j.1365-2443.2006.00945.x

Song, A., Labella, S., Korneeva, N. L., Keiper, B. D., Aamodt, E. J., Zetka, M. and Rhoads, R. E. (2010). A C. elegans eIF4E-family member upregulates translation at elevated temperatures of mRNAs encoding MSH-5 and other meiotic crossover proteins. *J. Cell Sci.* **123**, 2228-2237. doi:10.1242/jcs.063107

Spike, C. A., Coetzee, D., Nishi, Y., Guven-Ozkan, T., Oldenbroek, M., Yamamoto, I., Lin, R. and Greenstein, D. (2014). Translational control of the oogenic program by components of OMA ribonucleoprotein particles in Caenorhabditis elegans. *Genetics* **198**, 1513-1533. doi:10.1534/genetics.114.168823

Starostina, N. G., Lim, J.-M., Schvarzstein, M., Wells, L., Spence, A. M. and Kipreos, E. T. (2007). A CUL-2 ubiquitin ligase containing three FEM proteins degrades TRA-1 to regulate C. elegans sex determination. *Dev. Cell* **13**, 127-139. doi:10.1016/j.devcel.2007.05.008

Thompson, B. E., Bernstein, D. S., Bachorik, J. L., Petcherski, A. G., Wickens, M. and Kimble, J. (2005). Dose-dependent control of proliferation and sperm specification by FOG-1/CPEB. *Development* **132**, 3471-3481. doi:10.1242/dev.01921

Timmons, L. and Fire, A. (1998). Specific interference by ingested dsRNA [letter]. *Nature* **395**, 854. doi:10.1038/27579

Timmons, L., Court, D. L. and Fire, A. (2001). Ingestion of bacterially expressed dsRNAs can produce specific and potent genetic interference in *Caenorhabditis elegans*. *Gene* **263**, 103-112. doi:10.1016/S0378-1119(00)00579-5

Voronina, E., Paix, A. and Seydoux, G. (2012). The P granule component PGL-1 promotes the localization and silencing activity of the PUF protein FBF-2 in germline stem cells. *Development* **139**, 3732-3740. doi:10.1242/dev.083980

Wilhelm, J. E., Hilton, M., Amos, Q. and Henzel, W. J. (2003). Cup is an eIF4E binding protein required for both the translational repression of oskar and the recruitment of Barentsz. *J. Cell Biol.* **163**, 1197-1204. doi:10.1083/jcb.200309088

Yoon, D. S., Pendergrass, D. L. and Lee, M.-H. (2016). A simple and rapid method for combining fluorescent in situ RNA hybridization (FISH) and immunofluorescence in the C. elegans germline. *MethodsX* **3**, 378-385. doi:10.1016/j.mex.2016.05.001

Yoon, D. S., Alfhili, M. A., Friend, K. and Lee, M.-H. (2017). MPK-1/ERK regulatory network controls the number of sperm by regulating timing of sperm-oocyte switch in C. elegans germline. *Biochem. Biophys. Res. Commun.* **491**, 1077-1082. doi:10.1016/j.bbrc.2017.08.014

Yoon, D. S., Cha, D. S., Alfhili, M. A., Keiper, B. D. and Lee, M.-H. (2018). Subunits of the DNA polymerase alpha-primase complex promote Notch-mediated proliferation with discrete and shared functions in C. elegans germline. *FEBS J.* **285**, 2590-2604. doi:10.1111/febs.14512

Zahr, S. K., Yang, G., Kazan, H., Borrett, M. J., Yuzwa, S. A., Voronova, A., Kaplan, D. R. and Miller, F. D. (2018). A translational repression complex in developing mammalian neural stem cells that regulates neuronal specification. *Neuron* **97**, 520-537.e6. doi:10.1016/j.neuron.2017.12.045

Zanin, E., Pacquelet, A., Scheckel, C., Ciosk, R. and Gotta, M. (2010). LARP-1 promotes oogenesis by repressing fem-3 in the C. elegans germline. *J. Cell Sci.* **123**, 2717-2724. doi:10.1242/jcs.066761

Zhang, B., Gallegos, M., Puoti, A., Durkin, E., Fields, S., Kimble, J. and Wickens, M. P. (1997). A conserved RNA-binding protein that regulates sexual fates in the C. elegans hermaphrodite germ line. *Nature* **390**, 477-484. doi:10.1038/37297

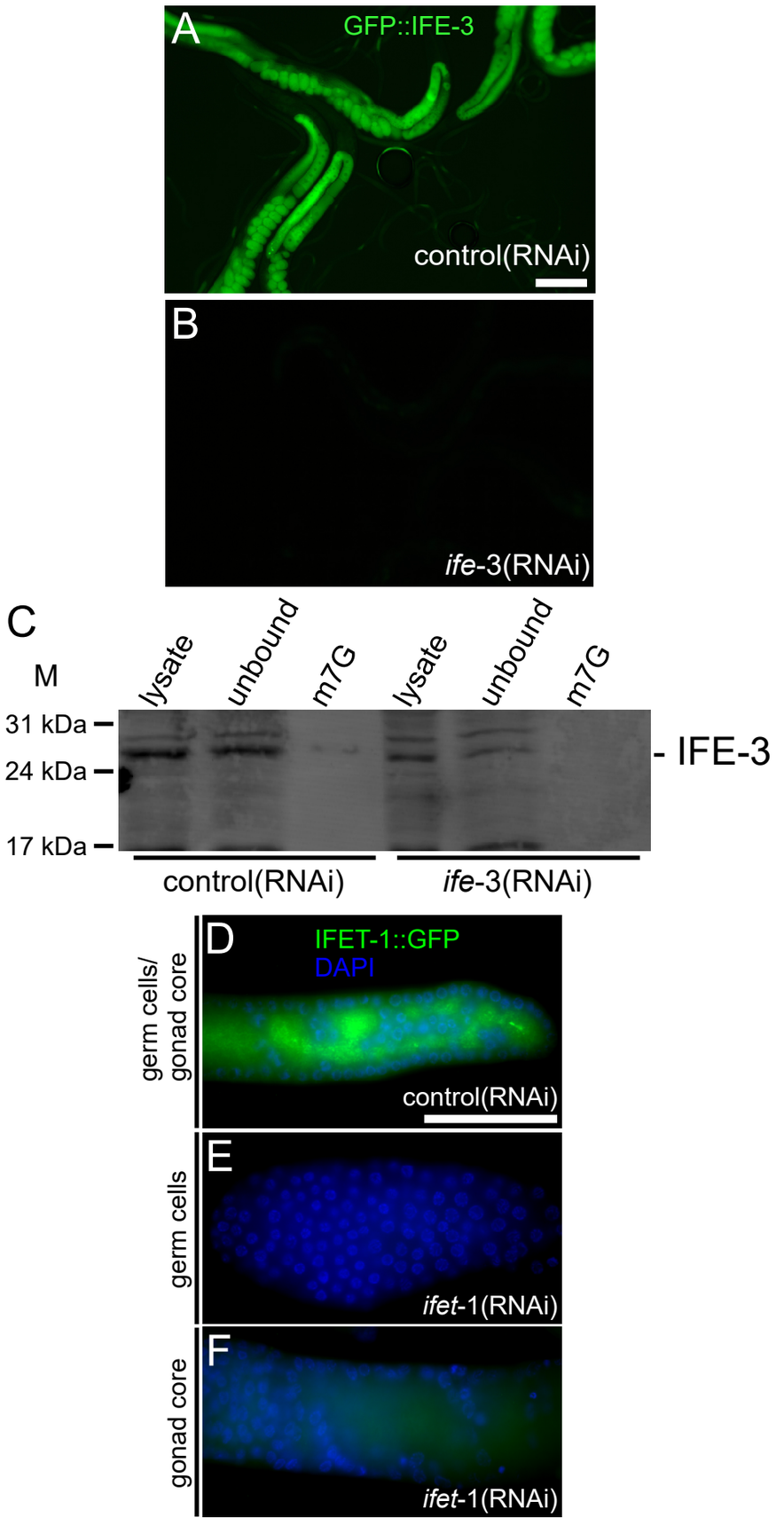

Figure S1. IFE-3 and IFET-1 depletion via RNAi. A) control(RNAi)-treated worms carrying *ife*-3(*eu21*[*gfp*::*tev*::3x*flag*::*ife*-3])V showing IFE-3 expression throughout the germline and in embryos. B) *ife*-3(RNAi)-treated worms carrying *ife*-3(*eu21*[*gfp*::*tev*::3x*flag*::*ife*-3])V showing IFE-3 depletion, as indicated by undetectable levels of GFP::IFE-3. C) Western blot analysis of wild type control(RNAi) and *ife*-3(RNAi)-treated worms showing IFE-3 depletion in the m^7G bound fraction of the *ife*-3(RNAi) lysate but not in the control(RNAi) lysate. IFE-3 was detected with primary antibody CA82 (Keiper et al., 2000). D) control(RNAi)-treated gonads carrying the *ifet*-1::*gfp::*3x*flag* transgene showing IFET-1 expression throughout the germline. E) *ifet*-1(RNAi)-treated gonad carrying *ifet*-1::*gfp::*3x*flag* showing loss of IFET-1::GFP from germ cells. F) *ifet*-1(RNAi)-treated gonad carrying *ifet*-1::*gfp::*3x*flag* showing IFET-1::GFP depletion in the rachis. These results confirm robust and specific IFE-3 and IFET-1 depletion upon *ife*-3(RNAi) and *ifet*-1(RNAi) treatments, respectively.

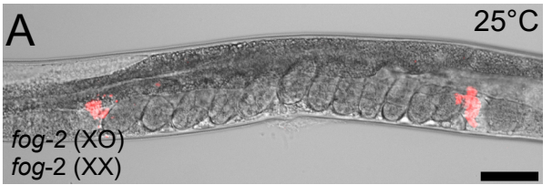

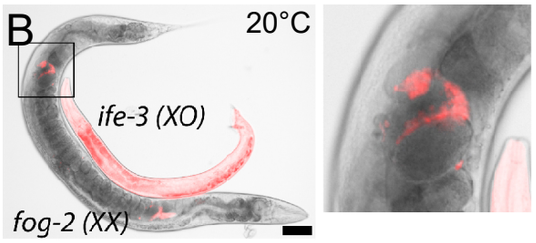

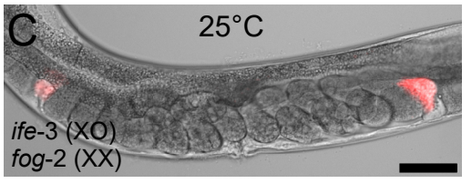

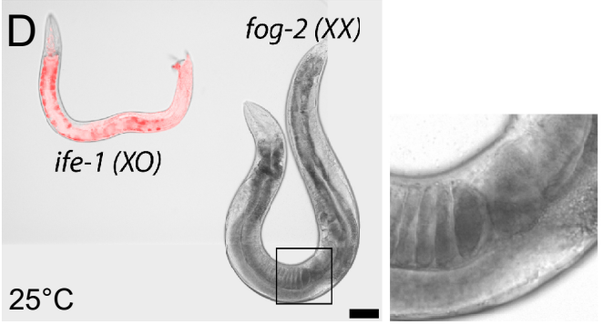

E

Male (XO)[a]	Female (XX)	n[b]	°C	Mating Efficiency (%)[c]	Fertility (%)[d]
fog-2	*fog*-2	12	20	83	100
fog-2	*fog*-2	10	25	40	100
ife-3	*fog*-2	10	20	80	100
ife-3	*fog*-2	20	25	15	100
ife-1	*fog*-2	10	20	70	100
ife-1	*fog*-2	10	25	0	0

[a] SYTO17 stained males
[b] 1:1 mating; genotype confirmed by genomic PCR
[c] Mating efficiency (%) = (# of SYTO17(+) fog-2 females/total # of fog-2 females) x 100
[d] Fertility (%) = (# of fertile fog-2 females/# of SYTO17(+) fog-2 females) x 100

Figure S2. SYTO17 staining of mutant males. A) *fog*-2(*q71*) female mated with SYTO17 stained *fog*-2(*q71*) male at 25°C showing efficient mating, as indicated by SYTO17(+) sperm in the spermatheca, and functionality of those sperm, as indicated by presence of embryos in the uterus. B) *fog*-2(*q71*) female mated with SYTO17 stained *ife*-3(-/-) male at 20°C showing efficient mating, as indicated by SYTO17(+) sperm in the spermatheca, and functionality of those sperm, as indicated by presence of embryos in the uterus. C) *fog*-2(*q71*) female mated with SYTO17 stained *ife*-3(-/-) male at 25°C showing efficient mating, as indicated by SYTO17(+) sperm in the spermatheca, and functionality of those sperm, as indicated by presence of embryos in the uterus. D) *fog*-2(*q71*) female mated with SYTO17 stained *ife*-1(-/-) male at 25°C showing inability of *ife*-1(-/-) males to produce sperm at elevated temperatures, as indicated by lack of SYTO17(+) sperm in the spermatheca and stacked oocytes in the absence of fertilization events.

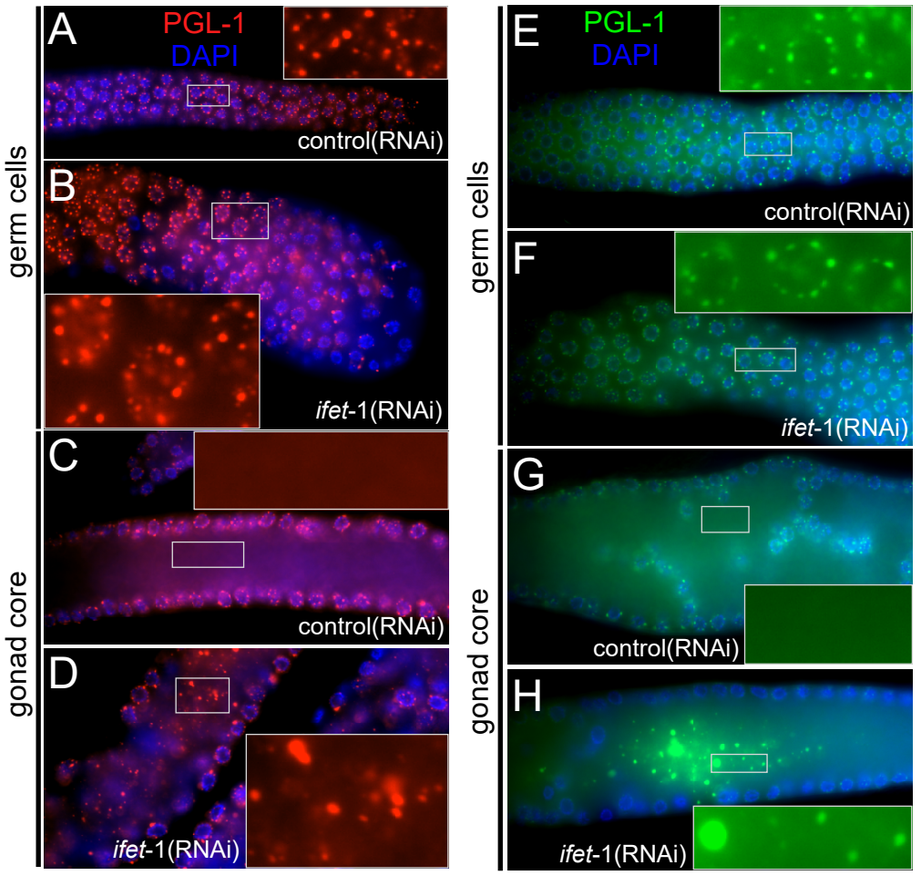

Figure S3. PGL-1 localization following IFET-1 depletion. A) PGL-1 (red) expression in animals treated with control(RNAi) shows that PGL-1 forms perinuclear granules in distal germ cells (inset, carats). B) PGL-1 expression in animals treated with *ifet*-1(RNAi) shows that perinuclear PGL-1 granules remain intact (inset). C) PGL-1 expression in animals treated with control(RNAi) shows that PGL-1 does not form structures in the gonad core (inset). D) PGL-1 expression in animals treated with *ifet*-1(RNAi) shows that PGL-1 accumulates into aggregates in the gonad core (inset). E) PGL-1 (green) expression in animals treated with control(RNAi) shows that PGL-1 forms perinuclear granules in distal germ cells (inset, carats). F) PGL-1 expression in animals treated with *ifet*-1(RNAi) shows that perinuclear PGL-1 granules remain intact (inset). G) PGL-1 expression in animals treated with control(RNAi) shows that PGL-1 does not form structures in the gonad core (inset). H) PGL-1 expression in animals treated with *ifet*-1(RNAi) shows that PGL-1 accumulates into aggregates in the gonad core (inset). These PGL-1 aggregates were found to be coincident with IFE-1 aggerates in the gonad core (see Fig. 8H). CRISPR/Cas9 fluorescently-tagged mKate2::TEV::3xmyc::IFE-1 and GFP::TEV::3xflag::IFE-3 were used to evaluate expression of endogenous IFEs. Similar CRISPR-tagged PGL-1 of the opposite color was used to track expression of endogenous PGL-1. Gonads were dissected, fixed, and counterstained (DAPI, blue) to visualize nuclear morphology. Scale bar: 50 μm.

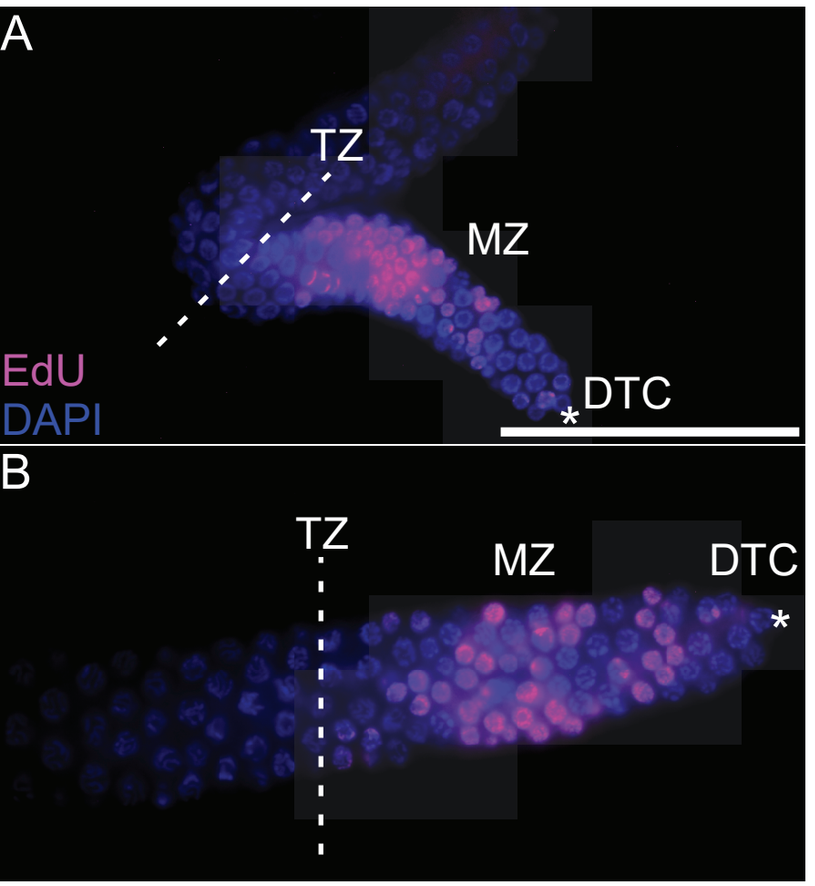

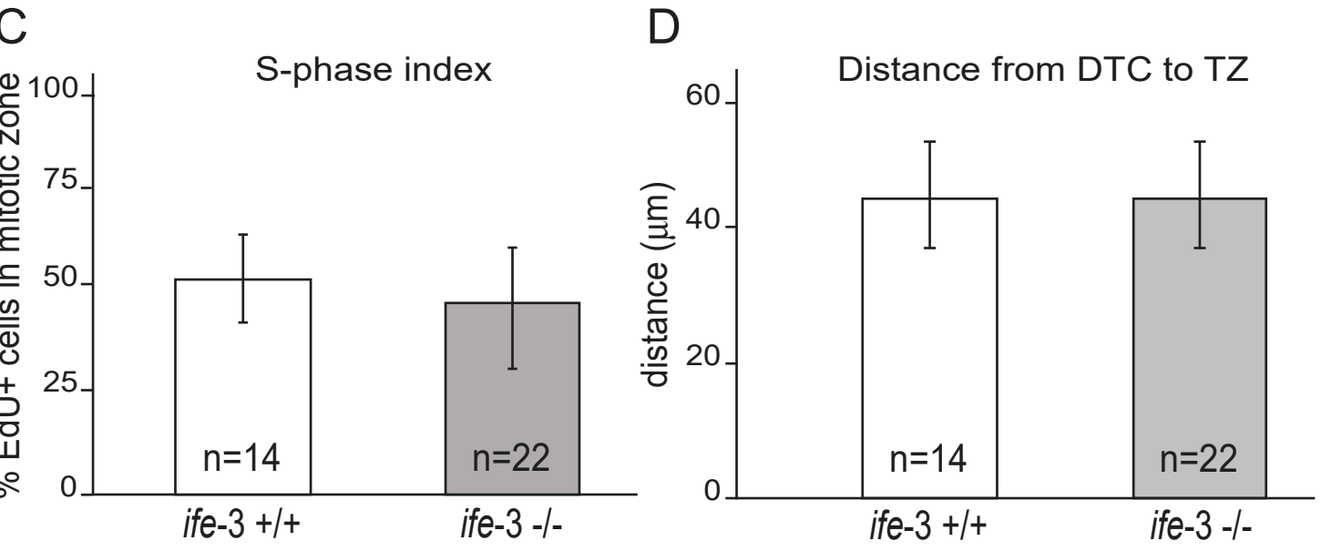

Figure S4. S-phase index and mitotic zone length in *ife*-3(*ok191*) animals. A) Wild type hermaphrodite gonad showing EdU (magenta) incorporation in germ cell that underwent S-phase. A) *ife*-3(-/-) hermaphrodite gonad showing EdU incorporation in germ cell that underwent S-phase, similar to what was seen for wild type. C) Quantification of S-phase indices and mitotic zone (MZ) length as measured from distal tip cell (DTC) to transition zone (TZ) in wild type (white) and *ife*-3(-/-) (grey) animals. No statically significant changes were seen in S-phase index or mitotic zone length in *ife*-3(-/-) animals compared to wildtype. Germlines of the indicated genotype were dissected, fixed, and counterstained with DAPI (blue) to visualize nuclear morphology. TZ was defined as the plane where at least two crescent shaped meiotic nuclei could be seen. Scale bar: 50 μm.

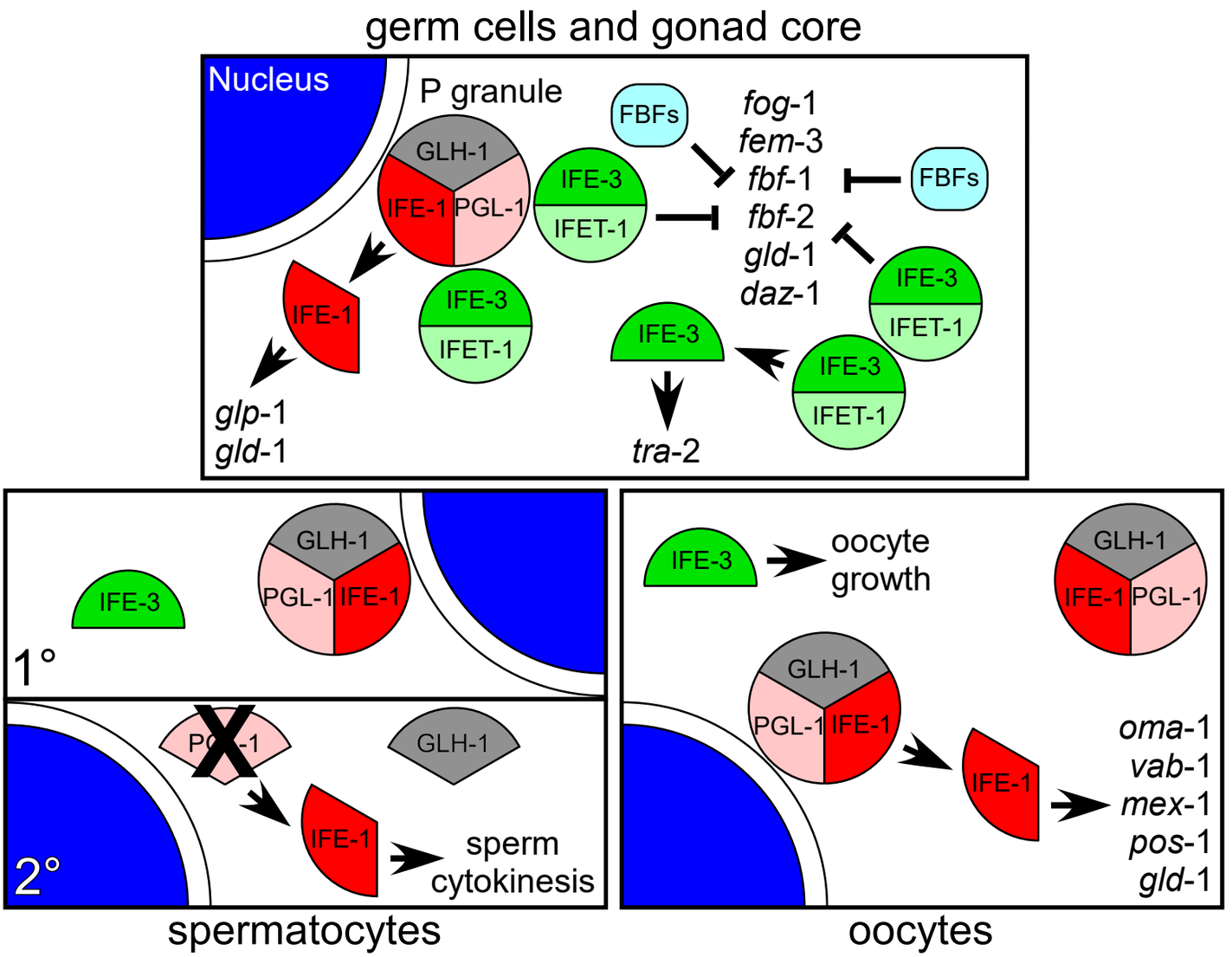

Figure S5. Model for differential spatial and temporal function of distinct eIF4E:4EBP complexes in the germline. Our findings demonstrate that loss of IFE-1 or IFE-3 cause very different germline phenotypes in *C. elegans*. These two eIF4E isoforms show different localization patterns, have different cognate 4EBPs, and translationally regulate different mRNAs. The model, based on this and other studies, is that IFE-1 and IFE-3 use their cognate 4EBPs to localize into unique germ granule mRNPs that presumably carry cargo mRNAs for translational repression. During germ cell development the IFE:4EBP mRNPs are remodeled to enter actively translating ribosomal complexes (see Fig. 1A). IFE-1 binds its 4EBP, PGL-1, directly and is the predominant P granule eIF4E. It promotes spermatocyte cytokinesis after leaving P granules in the latter stages of spermatogenesis and also positively regulates the translation of some maternal mRNAs which are also contained in P granules (*oma*-1, *vab*-1, *mex*-1, *pos*-1, *gld*-1). In contrast, IFE-3 is dispensable for spermatogenesis, and its major functions are in germline sex-determination (GSD), oocyte meiotic development and growth, and embryogenesis. IFE-3 also localizes to germ granules in the gonad, but they appear distinct from IFE-1:PGL-1 granules. IFET-1 binds IFE-3 directly, and controls its localization. We also provide evidence for hierarchical binding of IFET-1 to IFE-3, by showing that loss of IFE-3 has no effect on IFET-1 localization. IFE-3 ostensibly promotes oocyte fate by preventing translation of some GSD mRNAs (*fog*-1, *fem*-3, *fbf*-1, *fbf*-2, *gld*-1, *daz*-1) in conjuction with FBF proteins that are known to bind and repress GSD mRNAs. The role of IFE-3:IFET-1 may be to sequester these mRNAs to germ granles adjacent to P granules. The soluble portion of IFE-3 may activate the translation of *tra*-2 mRNA and other oocyte growth mRNAs consistent with its role in promoting oocyte fate. We propose that distinct eIF4E-4EBP-containing mRNPs in the germline are remodeled in response to developmental stimuli, which regulates the repression, activation, and degradation of mRNAs spatially and temporally throughout development.